Scattering of elastic waves by a sphere with cubic anisotropy with application to attenuation in polycrystalline materials

PROCEEDINGS A

royalsocietypublishing.org/journal/rspa

Research

Cite this article: Jafarzadeh A, Folkow PD, Boström A. 2023 Scattering of elastic waves by a sphere with cubic anisotropy with application to attenuation in polycrystalline materials. *Proc. R. Soc. A* **479**: 20220476. https://doi.org/10.1098/rspa.2022.0476

Received: 27 July 2022
Accepted: 21 March 2023

Subject Areas:
mechanical engineering, applied mathematics, wave motion

Keywords:
elastic wave scattering, cubic anisotropy, sphere, polycrystal, effective wavenumber

Author for correspondence:
Ata Jafarzadeh
e-mail: jata@chalmers.se

Scattering of elastic waves by a sphere with cubic anisotropy with application to attenuation in polycrystalline materials

Ata Jafarzadeh, Peter D. Folkow and Anders Boström

Department of Mechanics and Maritime Sciences, Chalmers University of Technology, Horsalsvagen 7, Gothenburg 412 96, Sweden

AJ, 0000-0003-3605-875X

Scattering of elastic waves by an anisotropic sphere with cubic symmetry inside an isotropic medium is studied. The waves in the isotropic surrounding are expanded in the spherical vector wave functions. Inside the sphere, the elastodynamic equations are first transformed to spherical coordinates and the displacement field is expanded in terms of the vector spherical harmonics in the angular directions and a power series in the radial direction. The governing equations inside the sphere give recursion relations among the expansion coefficients in the power series. The boundary conditions on the sphere then determine the expansion coefficients of the scattered wave. This determines the transition (**T**) matrix elements which are calculated explicitly to the leading order for low frequencies. Using the theory of Foldy, the **T** matrix elements of a single sphere are used to study attenuation and phase velocity of polycrystalline materials with cubic symmetry, explicitly for low frequencies and numerically for intermediate frequencies. Numerical comparisons of the present method with previously published results and recent finite element method (FEM) results show a good correspondence for low and intermediate frequencies. The present approach shows a better agreement with FEM for strongly anisotropic materials in comparison with other published methods.

Electronic supplementary material is available online at https://doi.org/10.6084/m9.figshare.c.6589814.

THE ROYAL SOCIETY PUBLISHING

1. Introduction

Scattering of elastic waves by a sphere started to receive attention from various disciplines of engineering and physical science in the mid-twentieth century [1]. These studies were continued with various applications, as in the investigation of dynamic stresses around cavities and rigid inclusions, the study of the propagation of ultrasonic pulses in crystalline alloys, non-destructive testing of different structures and geophysics. de Hoop [2] and Varadan *et al.* [3] present a comprehensive overview of wave scattering in two and three dimensions, which is not limited to elastic waves and covers electromagnetic and acoustic waves as well. These studies are limited to isotropic materials; however, there exist many synthetic (e.g. fibre composites) and natural (e.g. soils, rocks and grains in a metal) materials that are anisotropic. The governing equations of anisotropic materials are more complicated than for isotropic ones, making many of the analytical methods developed for isotropic materials not applicable anymore. Therefore, wave propagation in anisotropic materials has mostly been studied for unbounded and semi-bounded media in Cartesian and cylindrical coordinates. For finite obstacles, some authors have studied spherically and cylindrically anisotropic obstacles [4–8]. For bounded obstacles with anisotropy in Cartesian coordinates most studies have been performed for electromagnetic waves [9–11]. For mechanical waves, Boström studied two-dimensional scattering of elastic waves by an anisotropic circle [12,13]. In these studies, the displacement field inside the circle is expanded in trigonometric functions and a power series in the angular and radial coordinates, respectively. The same methodology is followed by Jafarzadeh *et al.* to study scattering by a transversely isotropic sphere, both for the special axisymmetric case involving only SH waves [14] and for the general case [15].

The scattering by a single obstacle is a first step when the scattering by two or more obstacles is investigated. Martin [16] presents an overview of different concepts followed by researchers to investigate interaction of time harmonic waves with multiple obstacles. A simple theory to study wave propagation through a medium having a distribution of obstacles is presented by Foldy [17] with the objective of characterizing the composite medium. In this theory, the effective wavenumber of the medium is estimated by the scattering coefficient of each obstacle, number density of obstacles and the wavenumber of the medium in the absence of any obstacles. Foldy developed this theory for scalar waves which, later on, was generalized to elastic waves [18,19]. Generalized Foldy theory, which is used by many authors to study wave propagation in an isotropic medium with isotropic inclusions [20,21], can be used to characterize grainy materials like polycrystalline materials [15].

Polycrystalline materials are solids consisting of many small crystals (the 'grains') which are normally anisotropic. In single phase polycrystalline materials, the lattice arrangement of atoms within each grain is nearly identical making the elastic constants identical for all grains. However, the orientation of the lattice is different for each grain. If the grains are equiaxed and randomly oriented in an infinite medium, the overall properties of the material become isotropic. The grainy nature of polycrystalline materials causes scattering and thus attenuation of the waves. To estimate the attenuation and the effective wave speed in polycrystals, these materials can be modelled in different ways such as a collection of individual particles, a regular array of particles and a stochastic process. Stanke & Kino [22] address different aspects of each geometrical model and use a stochastic process to estimate the attenuation and the phase velocity of polycrystalline materials with equiaxed anisotropic grains of cubic symmetry. Similar models of polycrystalline materials are further developed by researchers in various aspects. Explicit expressions for attenuation are presented using various approximate methods such as the Born approximation [23] and the far-field approximation (FFA) [24]. Different geometrical properties of the grains are captured for both equiaxed [24] and elongated [25] grains with a suitable introduction of a spatial two point correlation (TPC) function . Also different crystallographic classes are studied for crystals with hexagonal [26], orthorhombic [25] and triclinic [27] symmetry. It is shown that the anisotropy factor, which is a combination of the elastic constants of the material, is representative of the degree of anisotropy and the models lose their accuracy for materials with a high anisotropy factor. On the other hand, Boström & Ruda [28] in two dimensions looked at the polycrystalline

materials as a collection of individual grains in which each grain is considered to be surrounded by a matrix with the overall properties of all other grains (which is isotropic for equiaxed and randomly oriented grains). Using the explicit transition matrix for cubic materials presented by Boström [13], explicit expressions for the attenuation are derived for polycrystalline materials with cubic symmetry in two dimensions. With the same perspective, Jafarzadeh *et al.* [15] look at the polycrystalline materials as a special case of a distribution of inclusions and use the Foldy theory in combination with the **T** matrix of a single spherical obstacle to study attenuation and phase velocity of polycrystalline materials with hexagonal symmetry in three dimensions. Such an approach is only useful when the scattering by each grain is small, in particular for low frequencies. On the other hand, there seems to be no limitation on the degree of anisotropy.

Besides these analytical methods, Van Pamel *et al.* [29,30] present a finite element method (FEM) model for polycrystalline materials and investigate attenuation and phase velocity. This model is further developed for better accuracy and different material properties, and it is used as a reference for the development of analytical models [31–34].

The purpose of this paper is to find the **T** matrix elements for a spherical obstacle with cubic anisotropy (in Cartesian coordinates) in an isotropic surrounding and use them to characterize polycrystalline materials. The same methodology as for a spherical obstacle with transverse isotropy [15] is followed, the present case being more complicated in that there is no rotational symmetry any longer (leading to a coupling of different azimuthal orders). Stating the constitutive equations for a cubic material in spherical coordinates shows the complexity of the governing equations due to the appearance of explicit trigonometric functions in both the polar and azimuthal coordinates. For the transversely isotropic sphere studied by Jafarzadeh *et al.* [15] there is no trigonometric function in the azimuthal coordinate in the governing equations due to the rotational symmetry of the material. Using vector spherical harmonics and power series expansions in the angular and radial coordinates, respectively, the equations of motion lead to recursion relations for the coefficients in the power series expansion. Then the boundary conditions are applied and the **T** matrix elements for a single spherical obstacle are derived. These elements are used in combination with Foldy theory, and the attenuation and phase velocity of polycrystalline materials are calculated explicitly for low frequencies. Besides the explicit expression, a numerical calculation is also carried out and the attenuation and phase velocities are evaluated numerically for low and intermediate frequencies.

2. Statement of the problem

Scattering of elastic waves by an anisotropic sphere with radius a inside an infinite elastic homogeneous medium (figure 1) is considered. The surrounding medium is assumed isotropic with density ρ and Lamé parameters λ and μ. The material properties of the anisotropic sphere are described in the next section. Only monochromatic waves are studied and the time harmonic factor $\exp(-\mathrm{i}\omega t)$, where ω is the angular frequency and t is time, is suppressed. The longitudinal and transverse wave numbers of the infinite medium are $k_p^2 = \rho\omega^2/(\lambda + 2\mu)$ and $k_s^2 = \rho\omega^2/\mu$, respectively.

Based on the geometry of the inclusion it is natural to use spherical coordinates (r, θ, φ) and describe the field quantities in the surrounding medium with the aid of the spherical vector wave functions $\boldsymbol{\psi}_{\tau\sigma ml}$ introduced as [3]

$$\boldsymbol{\psi}^0_{1\sigma ml}(r,\theta,\varphi) = \frac{1}{\sqrt{l(l+1)}}\nabla \times (j_l(k_s r)Y_{\sigma ml}(\theta,\varphi)) = j_l(k_s r)\boldsymbol{A}_{1\sigma ml}(\theta,\varphi), \tag{2.1}$$

$$\boldsymbol{\psi}^0_{2\sigma ml}(r,\theta,\varphi) = \frac{1}{\sqrt{l(l+1)}}\frac{1}{k_s}\nabla \times \nabla \times (j_l(k_s r)Y_{\sigma ml}(\theta,\varphi))$$

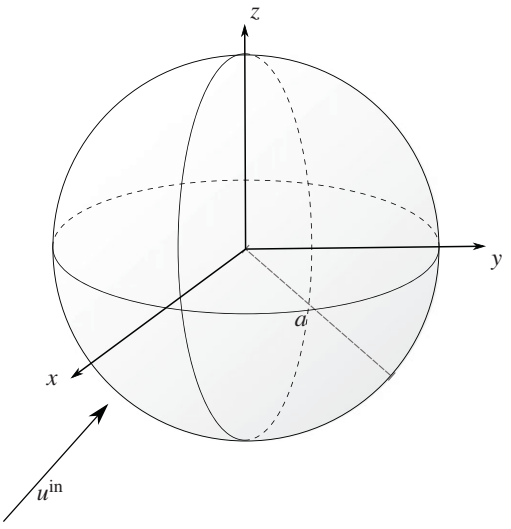

Figure 1. The cubic sphere with radius a and the incident wave u^{in}.

$$= \left(j_l'(k_s r) + \frac{j_l(k_s r)}{k_s r} \right) \boldsymbol{A}_{2\sigma ml}(\theta, \varphi) + \sqrt{l(l+1)} \frac{j_l(k_s r)}{k_s r} \boldsymbol{A}_{3\sigma ml}(\theta, \varphi) \tag{2.2}$$

and

$$\boldsymbol{\psi}^0_{3\sigma ml}(r, \theta, \varphi) = \left(\frac{k_p}{k_s} \right)^{3/2} \frac{1}{k_p} \nabla (j_l(k_p r) Y_{\sigma ml}(\theta, \varphi))$$

$$= \left(\frac{k_p}{k_s} \right)^{3/2} \left((j_l'(k_p r) \boldsymbol{A}_{3\sigma ml}(\theta, \varphi) + \sqrt{l(l+1)} \frac{j_l(k_p r)}{k_p r} \boldsymbol{A}_{2\sigma ml}(\theta, \varphi) \right). \tag{2.3}$$

The type of the wave function is specified by the first index $\tau = 1, 2, 3$ for SH, SV and P waves, respectively. The other indices are running through $m = 0, 1, \ldots, l = m, m+1, \ldots$ and $\sigma = e$ (even) and o (odd). $l = 0$ is only relevant for the P wavefunctions ($\tau = 3$) and is not defined for the others. The upper index '0' on the wave functions denotes that they are regular and contain spherical Bessel functions. The corresponding outgoing wave functions are denoted by the upper index '+' and contain spherical Hankel functions to fulfil the radiation condition. $\boldsymbol{A}_{\tau\sigma ml}(\theta, \varphi)$ are vector spherical harmonics which constitute a complete orthonormal vector basis system on the unit sphere for vector valued functions and are defined as

$$\left.\begin{aligned} \boldsymbol{A}_{1\sigma ml}(\theta, \varphi) &= \frac{1}{\sqrt{l(l+1)}} \nabla \times (\boldsymbol{r} Y_{\sigma ml}(\theta, \varphi)) \\ &= \frac{1}{\sqrt{l(l+1)}} \left(\boldsymbol{e}_\theta \frac{1}{\sin\theta} \frac{\partial}{\partial \varphi} Y_{\sigma ml}(\theta, \varphi) - \boldsymbol{e}_\varphi \frac{\partial}{\partial \theta} Y_{\sigma ml}(\theta, \varphi) \right), \\ \boldsymbol{A}_{2\sigma ml}(\theta, \varphi) &= \frac{1}{\sqrt{l(l+1)}} r \nabla Y_{\sigma ml}(\theta, \varphi) \\ &= \frac{1}{\sqrt{l(l+1)}} \left(\boldsymbol{e}_\theta \frac{\partial}{\partial \theta} Y_{\sigma ml}(\theta, \varphi) + \boldsymbol{e}_\varphi \frac{1}{\sin\theta} \frac{\partial}{\partial \varphi} Y_{\sigma ml}(\theta, \varphi) \right) \end{aligned}\right\} \tag{2.4}$$

and

$$\boldsymbol{A}_{3\sigma ml}(\theta, \varphi) = \boldsymbol{e}_r Y_{\sigma ml}(\theta, \varphi),$$

in which $Y_{\sigma ml}(\theta, \varphi)$ are spherical harmonics with the following definition

$$Y_{\sigma ml}(\theta, \varphi) = \sqrt{\frac{\epsilon_m (2l+1)(l-m)!}{4\pi (l+m)!}} P_l^m(\cos\theta) \begin{Bmatrix} \cos m\varphi \\ \sin m\varphi \end{Bmatrix}. \tag{2.5}$$

Here, $P_l^m(\cos\theta)$ is an associated Legendre function of order m and degree l. The Neumann factor is ϵ_m with $\epsilon_0 = 1$ and $\epsilon_m = 2$ for $m = 1, 2, \ldots$. Also, $\sigma = e$ is for the upper row which is even with respect to φ and $\sigma = o$ is for the lower row which is odd with respect to φ. The φ-dependence of the wave functions is often expressed as the complex exponential $e^{im\varphi}$ instead, but here it is more convenient to use the trigonometric functions $\cos m\varphi$ and $\sin m\varphi$ as these are even and odd, respectively, and this is useful for subdividing the scattering problem into parts depending on the symmetries.

These wave functions are sufficient to describe the displacement field in an isotropic medium in spherical coordinates. The radial traction on the boundary of the sphere is also needed for the boundary conditions. It is convenient to introduce the radial traction operator in an isotropic medium

$$\boldsymbol{t}^{(r)} = \boldsymbol{e}_r \lambda \nabla \cdot \boldsymbol{u} + \mu \left(2\frac{\partial \boldsymbol{u}}{\partial r} + \boldsymbol{e}_r \times (\nabla \times \boldsymbol{u}) \right), \tag{2.6}$$

and derive the corresponding traction for each of the vector wave functions as

$$\boldsymbol{t}^{(r)}(\boldsymbol{\psi}^0_{1\sigma ml}(\boldsymbol{r})) = \mu r \frac{\mathrm{d}}{\mathrm{d}r}\left(\frac{j_l(k_s r)}{r}\right) \boldsymbol{A}_{1\sigma ml}(\theta, \varphi), \tag{2.7}$$

$$\begin{aligned} \boldsymbol{t}^{(r)}(\boldsymbol{\psi}^0_{2\sigma ml}(\boldsymbol{r})) = \mu \Bigg[& \left(2k_s j_l''(k_s r) + \frac{2j_l'(k_s r)}{r} - \frac{2j_l(k_s r)}{k_s r^2} + k_s j_l(k_s r) \right) \boldsymbol{A}_{2\sigma ml}(\theta, \varphi) \\ & + 2\sqrt{l(l+1)} \frac{\mathrm{d}}{\mathrm{d}r}\left(\frac{j_l(k_s r)}{k_s r}\right) \boldsymbol{A}_{3\sigma ml}(\theta, \varphi) \Bigg] \end{aligned} \tag{2.8}$$

and

$$\begin{aligned} \boldsymbol{t}^{(r)}(\boldsymbol{\psi}^0_{3\sigma ml}(\boldsymbol{r})) = \mu \left(\frac{k_p}{k_s}\right)^{3/2} \Bigg[& \left((2k_p j_l''(k_p r) + \frac{2k_p^2 - k_s^2}{k_p} j_l(k_p r) \right) \\ & \times \boldsymbol{A}_{3\sigma ml}(\theta, \varphi) + 2\sqrt{l(l+1)} \frac{\mathrm{d}}{\mathrm{d}r}\left(\frac{j_l(k_p r)}{k_p r}\right) \boldsymbol{A}_{2\sigma ml}(\theta, \varphi) \Bigg]. \end{aligned} \tag{2.9}$$

Assuming that the sources of the incident wave are located outside the sphere, then close enough to the sphere the incident displacement field can be expanded in terms of the regular wave functions

$$\boldsymbol{u}^{\mathrm{in}}(\boldsymbol{r}) = \sum_{\tau\sigma ml} b_{\tau\sigma ml} \boldsymbol{\psi}^0_{\tau\sigma ml}(\boldsymbol{r}), \tag{2.10}$$

where the indices run through $\tau = 1, 2, 3$, $\sigma = e, o$, $m = 0, 1, \ldots, l = m, m+1, \ldots$, and the expansion coefficients of the incident wave $b_{\tau\sigma ml}$ are in principle known. The incident wave is scattered by the sphere and this leads to an outgoing scattered wave. The scattered wave must satisfy radiation conditions and can be expanded in terms of the outgoing wave functions

$$\boldsymbol{u}^{sc}(\boldsymbol{r}) = \sum_{\tau\sigma ml} h_{\tau\sigma ml} \boldsymbol{\psi}^+_{\tau\sigma ml}(\boldsymbol{r}). \tag{2.11}$$

Here, $h_{\tau\sigma ml}$ are the unknown scattered wave coefficients which are to be determined. A general way to represent the scattering by an obstacle is to determine the transition matrix (**T** matrix) which gives the linear relation between the expansion coefficients of the incident and scattered waves

$$h_{\tau\sigma ml} = \sum_{\tau'\sigma'm'l'} T_{\tau\sigma ml,\tau'\sigma'm'l'} b_{\tau'\sigma'm'l'}. \tag{2.12}$$

This completes the necessary developments in the surrounding medium to solve the scattering problem. In the following sections, the anisotropic sphere is described and the transition matrix elements are derived.

3. The cubic sphere

In this section, the material properties and governing equations of the anisotropic sphere are discussed. The sphere has density ρ_1 and is anisotropic with cubic properties. A cubic material can be defined by three independent stiffness constants, here denoted C_{11}, C_{12} and C_{44} in abbreviated notation. The constitutive relations can then be expressed in Cartesian coordinates

$$\begin{Bmatrix} \sigma_{xx} \\ \sigma_{yy} \\ \sigma_{zz} \\ \sigma_{yz} \\ \sigma_{zx} \\ \sigma_{xy} \end{Bmatrix} = \begin{bmatrix} C_{11} & C_{12} & C_{12} & 0 & 0 & 0 \\ C_{12} & C_{11} & C_{12} & 0 & 0 & 0 \\ C_{12} & C_{12} & C_{11} & 0 & 0 & 0 \\ 0 & 0 & 0 & 2C_{44} & 0 & 0 \\ 0 & 0 & 0 & 0 & 2C_{44} & 0 \\ 0 & 0 & 0 & 0 & 0 & 2C_{44} \end{bmatrix} \begin{Bmatrix} \epsilon_{xx} \\ \epsilon_{yy} \\ \epsilon_{zz} \\ \epsilon_{yz} \\ \epsilon_{zx} \\ \epsilon_{xy} \end{Bmatrix}. \tag{3.1}$$

Considering the geometry of the problem it is more convenient to express the stress–strain relations in spherical coordinates. Transforming the constitutive relation in equation (3.1) to spherical coordinates (see [15]) the stress–strain relations in spherical coordinates become

$$\begin{aligned}
\sigma_{rr} &= (\alpha_1 + 2\alpha_2)\epsilon_{rr} + \alpha_1\epsilon_{\theta\theta} + \left(\alpha_1 - \frac{3}{4}\beta\right)\epsilon_{\varphi\varphi} \\
&\quad + \beta\Bigg[\sin 4\varphi\big((\cos\theta - \cos 3\theta)\epsilon_{\theta\varphi} + (3\sin\theta - \sin 3\theta)\epsilon_{\varphi r}\big) \\
&\quad + \cos 4\varphi\left(\frac{3}{4}\epsilon_{rr} + \frac{1}{4}\epsilon_{\theta\theta} - \epsilon_{\varphi\varphi} + \cos 2\theta(\epsilon_{\phi\phi} - \epsilon_{rr})\right. \\
&\quad + \frac{1}{4}\cos 4\theta(\epsilon_{rr} - \epsilon_{\theta\theta}) + \left(\sin 2\theta - \frac{1}{2}\sin 4\theta\right)\epsilon_{r\theta}\Big) + \cos 2\theta(\epsilon_{rr} - \epsilon_{\varphi\varphi}) \\
&\quad + \frac{7}{4}\cos 4\theta(\epsilon_{rr} - \epsilon_{\theta\theta}) - \left(\sin 2\theta + \frac{7}{2}\sin 4\theta\right)\epsilon_{r\theta}\Bigg],
\end{aligned} \tag{3.2}$$

$$\begin{aligned}
\sigma_{\theta\theta} &= \alpha_1\epsilon_{rr} + (\alpha_1 + 2\alpha_2)\epsilon_{\theta\theta} + \left(\alpha_1 - \frac{3}{4}\beta\right)\epsilon_{\varphi\varphi} \\
&\quad + \beta\Bigg[\sin 4\varphi\big((3\cos\theta + \cos 3\theta)\epsilon_{\theta\varphi} + (\sin\theta + \sin 3\theta)\epsilon_{\varphi r}\big) \\
&\quad + \cos 4\varphi\left(\frac{1}{4}\epsilon_{rr} + \frac{3}{4}\epsilon_{\theta\theta} - \epsilon_{\varphi\varphi} - \cos 2\theta(\epsilon_{\phi\phi} - \epsilon_{\theta\theta})\right. \\
&\quad - \frac{1}{4}\cos 4\theta(\epsilon_{rr} - \epsilon_{\theta\theta}) + \left(\sin 2\theta + \frac{1}{2}\sin 4\theta\right)\epsilon_{r\theta}\Big) - \cos 2\theta(\epsilon_{\theta\theta} - \epsilon_{\varphi\varphi}) \\
&\quad - \frac{7}{4}\cos 4\theta(\epsilon_{rr} - \epsilon_{\theta\theta}) - \left(\sin 2\theta - \frac{7}{2}\sin 4\theta\right)\epsilon_{r\theta}\Bigg],
\end{aligned} \tag{3.3}$$

$$\begin{aligned}
\sigma_{\varphi\varphi} &= \left(\alpha_1 - \frac{3}{4}\beta\right)\epsilon_{rr} + \left(\alpha_1 - \frac{3}{4}\beta\right)\epsilon_{\theta\theta} + \left(\alpha_1 + 2\alpha_2 + \frac{3}{4}\beta\right)\epsilon_{\varphi\varphi} \\
&\quad + \beta\Bigg[\cos 2\theta(\epsilon_{\theta\theta} - \epsilon_{rr}) + 2\sin 2\theta\epsilon_{r\theta} \\
&\quad + \cos 4\varphi(2\epsilon_{\varphi\varphi} - \epsilon_{rr} - \epsilon_{\theta\theta} + \cos 2\theta(\epsilon_{rr} - \epsilon_{\theta\theta}) - 2\sin 2\theta\epsilon_{r\theta}) \\
&\quad + 4\sin 4\varphi(\cos\theta\epsilon_{\theta\varphi} + \sin\theta\epsilon_{\varphi r})\Bigg],
\end{aligned} \tag{3.4}$$

$$\begin{aligned}
\sigma_{r\theta} &= (2\alpha_2)\epsilon_{r\theta} + \frac{1}{2}\beta\Bigg[-7\cos 4\theta\epsilon_{r\theta} + \sin 2\theta(2\epsilon_{\varphi\varphi} - \epsilon_{rr} - \epsilon_{\theta\theta}) \\
&\quad + \frac{7}{2}\sin 4\theta(\epsilon_{\theta\theta} - \epsilon_{rr}) + \cos 4\varphi(\epsilon_{r\theta} - \cos 4\theta\epsilon_{r\theta}
\end{aligned}$$

$$+\sin 2\theta(\epsilon_{rr}+\epsilon_{\theta\theta}-2\epsilon_{\varphi\varphi})+\frac{1}{2}\sin 4\theta(\epsilon_{\theta\theta}-\epsilon_{rr})\Big)$$
$$-2\sin 4\varphi((\cos\theta-\cos 3\theta)\epsilon_{\varphi r}+(\sin\theta+\sin 3\theta)\epsilon_{\theta\varphi})\Big], \tag{3.5}$$

$$\sigma_{\theta\varphi}=\left(2\alpha_2-\frac{3}{2}\beta\right)\epsilon_{\varphi r}+2\beta\Big[-\cos 2\theta\epsilon_{\varphi r}+\sin 2\theta\epsilon_{\theta\varphi}$$
$$-\cos 4\varphi((1-\cos 2\theta)\epsilon_{\varphi r}+\sin 2\theta\epsilon_{\theta\varphi})+\frac{1}{2}\sin 4\varphi\Big((\cos 3\theta-\cos\theta)\epsilon_{r\theta}$$
$$+\sin\theta\left(2\epsilon_{\varphi\varphi}-\frac{3}{2}\epsilon_{rr}-\frac{1}{2}\epsilon_{\theta\theta}\right)+\frac{1}{2}\sin 3\theta(\epsilon_{rr}-\epsilon_{\theta\theta})\Big)\Big] \tag{3.6}$$

and
$$\sigma_{\varphi r}=\left(2\alpha_2-\frac{3}{2}\beta\right)\epsilon_{\theta\varphi}+2\beta\Big[\cos 2\theta\epsilon_{\theta\varphi}+\sin 2\theta\epsilon_{\varphi r}-\cos 4\varphi((1+\cos 2\theta)\epsilon_{\theta\varphi}+\sin 2\theta\epsilon_{\varphi r})$$
$$+\frac{1}{2}\sin 4\varphi\Big(\cos\theta\left(2\epsilon_{\varphi\varphi}-\frac{1}{2}\epsilon_{rr}-\frac{3}{2}\epsilon_{\theta\theta}\right)+\frac{1}{2}\cos 3\theta(\epsilon_{rr}-\epsilon_{\theta\theta})-(\sin\theta+\sin 3\theta)\epsilon_{r\theta}\Big)\Big], \tag{3.7}$$

where the strains in spherical coordinates are

$$\left.\begin{aligned}
&\epsilon_{rr}=\frac{\partial u_r}{\partial r},\quad \epsilon_{\varphi\varphi}=\frac{1}{r\sin\theta}\frac{\partial u_\varphi}{\partial\varphi}+\frac{\cot\theta}{r}u_\theta+\frac{u_r}{r},\\
&\epsilon_{\theta\theta}=\frac{1}{r}\frac{\partial u_\theta}{\partial\theta}+\frac{u_r}{r},\quad \epsilon_{\theta\varphi}=\frac{1}{2r}\left(\frac{\partial u_\varphi}{\partial\theta}-\cot\theta u_\varphi+\frac{1}{\sin\theta}\frac{\partial u_\theta}{\partial\varphi}\right)\\
&\epsilon_{\varphi r}=\frac{1}{2}\left(\frac{1}{r\sin\theta}\frac{\partial u_r}{\partial\varphi}+\frac{\partial u_\varphi}{\partial r}-\frac{u_\varphi}{r}\right),\quad\text{and}\quad \epsilon_{r\theta}=\frac{1}{2}\left(\frac{\partial u_\theta}{\partial r}-\frac{u_\theta}{r}+\frac{1}{r}\frac{\partial u_r}{\partial\theta}\right).
\end{aligned}\right\} \tag{3.8}$$

Here, α_1, α_2 and β are new stiffness constants defined by

$$\left.\begin{aligned}
&\alpha_1=\frac{1}{32}(7C_{11}+25C_{12}-14C_{44}),\quad \alpha_2=\frac{1}{32}(7C_{11}-7C_{12}+18C_{44})\\
&\text{and}\qquad \beta=\frac{1}{8}(C_{11}-C_{12}-2C_{44}).
\end{aligned}\right\} \tag{3.9}$$

In the isotropic limit, when $C_{44}=(C_{11}-C_{12})/2$, it can be observed that $\beta=0$, $\alpha_1=\lambda_1$ and $\alpha_2=\mu_1$, where λ_1 and μ_1 are Lamé parameters of an isotropic sphere.

Besides the stress–strain relations inside the sphere, the governing equations can also be expressed in spherical coordinates as

$$\frac{\partial\sigma_{rr}}{\partial r}+\frac{1}{r}\frac{\partial\sigma_{r\theta}}{\partial\theta}+\frac{1}{r\sin\theta}\frac{\partial\sigma_{\varphi r}}{\partial\varphi}+\frac{1}{r}(2\sigma_{rr}-\sigma_{\theta\theta}-\sigma_{\varphi r}+\cot\theta\sigma_{r\theta})+\rho\omega^2u_r=0, \tag{3.10}$$

$$\frac{\partial\sigma_{r\theta}}{\partial r}+\frac{1}{r}\frac{\partial\sigma_{\theta\theta}}{\partial\theta}+\frac{1}{r\sin\theta}\frac{\partial\sigma_{\theta\varphi}}{\partial\varphi}+\frac{1}{r}(\cot\theta(\sigma_{\theta\theta}-\sigma_{\varphi\varphi})+3\sigma_{r\theta})+\rho\omega^2u_\theta=0 \tag{3.11}$$

and
$$\frac{\partial\sigma_{\varphi r}}{\partial r}+\frac{1}{r}\frac{\partial\sigma_{\theta\varphi}}{\partial\theta}+\frac{1}{r\sin\theta}\frac{\partial\sigma_{\varphi\varphi}}{\partial\varphi}+\frac{1}{r}(3\sigma_{\varphi r}+2\cot\theta\sigma_{\theta\varphi})+\rho\omega^2u_\varphi=0. \tag{3.12}$$

Of course, these governing equations can be expressed in terms of the displacements; however, this leads to very large equations which are not given.

To solve the scattering problem, the scattered wave outside the sphere and the wave inside the sphere need to be determined given the incident wave. In equation (2.11), the scattered wave is expanded in terms of the spherical vector wave functions. However, these wave functions are not a solution of the elastodynamic equations of an anisotropic medium expressed in equations (3.10)–(3.12) and the displacement field inside the sphere cannot be expressed in terms of these vector wave functions. However, the vector spherical harmonics constitute a complete orthonormal vector basis system for vector valued functions which is suitable for the expansion of the displacement inside the sphere since the displacement and stress fields outside the sphere are

also in terms of the vector spherical harmonics and this facilitates the application of the boundary conditions. Consequently, the displacement field $\boldsymbol{u}_1$ inside the sphere is expanded as

$$\boldsymbol{u}_1(r,\theta,\varphi)=\sum_{\tau\sigma ml} F_{\tau\sigma ml}(r)\boldsymbol{A}_{\tau\sigma ml}(\theta,\varphi), \tag{3.13}$$

where $l=1,2,\ldots$ for $\tau=1,2$ and $l=0,1,\ldots$ for $\tau=3$. The r-dependent coefficients $F_{\tau\sigma ml}(r)$ are expanded in power series in r. By considering the regularity condition at the centre of the sphere when $r\to 0$, these expansions are

$$F_{1\sigma ml}(r)=\sum_{j=l,l+2,\ldots}^{\infty} f_{1\sigma ml,j}r^j, \tag{3.14}$$

$$F_{2\sigma ml}(r)=\sum_{j=l-1,l+1,\ldots}^{\infty} f_{2\sigma ml,j}r^j \tag{3.15}$$

and

$$F_{3\sigma ml}(r)=\sum_{j=l-1,l+1,\ldots}^{\infty} f_{3\sigma ml,j}r^j, \tag{3.16}$$

in which $f_{3\sigma m0,-1}=0$. Here, $f_{\tau\sigma ml,j}$ are the unknown coefficients inside the sphere. The scattering problem can be addressed as finding these coefficients together with the unknown coefficients of the scattered wave $h_{\tau\sigma ml}$. To do so, the governing equations (equations (3.10)–(3.12)) are used to derive recursion relations among the unknown coefficients. Then the boundary conditions for the displacement and traction are used to find all the rest of the unknown coefficients.

In order to find the recursion relations among the unknown coefficients the governing equations (equations (3.10)–(3.12)) are considered as a vector valued function which is expanded in terms of the vector spherical harmonics

$$\sum_{\tau\sigma ml} H_{\tau\sigma ml}(r)\boldsymbol{A}_{\tau\sigma ml}(\theta,\varphi)=\boldsymbol{0}. \tag{3.17}$$

The orthogonality of the vector spherical harmonics means that all the coefficients must vanish

$$H_{\tau\sigma ml}(r)=0 \quad \text{for all } \tau,\sigma,m,l. \tag{3.18}$$

These equations are power series in r, but as the powers of r are linearly independent, the coefficient in front of every power of r must vanish and this provides recursion relations among the unknown coefficients inside the sphere. The general explicit expression of the recursion relations is complicated and is not given; however, it is enlightening to state how $H_{\tau\sigma ml}$ depends on the unknown expansion coefficients $f_{\tau\sigma ml,j}$. In the isotropic case there is only coupling between P and SV waves meaning that $H_{1\sigma ml}$ contains $f_{1\sigma ml,j}$ and $H_{\tau\sigma ml}$ contains $f_{\tau'\sigma ml,j}$ where τ and τ' can be 2 and 3. On the other hand, for a sphere with cubic symmetry, the trigonometric functions of different orders with respect to θ and φ, which appear in the stress–strain relations in spherical coordinates (equations (3.2)–(3.7)), lead to coupling between different values of m and l. Specifically, $H_{1\sigma ml}$ may contain $f_{1\sigma m'l',j}$ where m' can be m and $|m\pm 4|$, and l' can be $l, l\pm 2$. For P–SV waves $H_{\tau\sigma ml}$ may contain $f_{\tau'\sigma m'l',j}$ where τ and τ' can be 2 and 3, m' can be m and $|m\pm 4|$ and l' can be $l, l\pm 2$ and $l\pm 4$. Beside such coupling, there is also coupling between SH waves and P–SV waves. Such coupling occurs with different parity of SH and P–SV waves with respect to θ and φ (for l and σ values). This can be observed in equations (2.1)–(2.5) where the displacement field has the same parity for all components if the SH waves ($\boldsymbol{\psi}_{1\sigma ml}$) have a different parity compared to P–SV waves ($\boldsymbol{\psi}_{2\sigma ml}$ and $\boldsymbol{\psi}_{3\sigma ml}$) with respect to θ (l values) and φ (σ values). This means $H_{1\sigma ml}$ may contain $f_{\tau\sigma'm'l',j}$ and $H_{\tau\sigma ml}$ may contain $f_{1\sigma'm'l',j}$ in which τ can be 2 and 3, $\sigma\neq\sigma'$, m' can be m and $|m\pm 4|$ and l' can be $l\pm 1$ and $l\pm 3$. The reason for the absolute value in coupling between different m values is the fact that negative orders of trigonometric functions and associated Legendre functions are essentially the same as the ones with positive orders. This means that coupling between $m=1$ and $m=-3$ is equivalent with coupling between $m=1$ and

Table 1. Table of coupling among partial waves in the Rayleigh limit.

	P–SV				
m	σl	partial P waves	partial SV waves	partial SH waves	sec.
0,4	ee	$A_{3e00}, A_{3e02}, (A_{3e04}, A_{3e44})$	$A_{2e02}, (A_{2e04}, A_{2e44})$	—	4(a)
	eo	$A_{3e01}, (A_{3e03})$	$A_{2e01}, (A_{2e03})$	—	4(b)
	oe	(A_{3o44})	(A_{2o44})	$A_{1e01}, (A_{1e03})$	4(c)
	oo	—	—	A_{1e02}	4(c)
1,3	ee	$A_{3e12}, (A_{3e14}, A_{3e34})$	$A_{2e12}, (A_{2e14}, A_{2e34})$	$A_{1o11}, (A_{1o13}, A_{1o33})$	5(a)
	eo	$A_{3e11}, (A_{3e13}, A_{3e33})$	$A_{2e11}, (A_{2e13}, A_{2e33})$	A_{1o12}	5(b)
	oe	$A_{3o12}, (A_{3o14}, A_{3o34})$	$A_{2o12}, (A_{2o14}, A_{2o34})$	$A_{1e11}, (A_{1e13}, A_{1e33})$	5(a)
	oo	$A_{3o11}, (A_{3o13}, A_{3o33})$	$A_{2o11}, (A_{2o13}, A_{2o33})$	A_{1e12}	5(b)
2	ee	$A_{3e22}, (A_{3e24})$	$A_{2e22}, (A_{2e24})$	(A_{1o23})	6(a)
	eo	(A_{3e23})	(A_{2e23})	A_{1o22}	—
	oe	$A_{3o22}, (A_{3o24})$	$A_{2o22}, (A_{2o24})$	(A_{1e23})	6(b)
	oo	(A_{3o23})	(A_{2o23})	A_{1e22}	—

$m=3$, while $l=1$ is not coupled with $l=-1$ and $l=-3$, since a negative degree of the associated Legendre functions is not defined.

Finally, to find the remaining unknown coefficients inside the sphere ($f_{\tau\sigma ml,j}$) and the unknown scattered wave expansion coefficients outside the sphere ($h_{\tau\sigma ml}$), the boundary conditions must be applied. For a welded spherical obstacle this can be stated as continuity of the displacement and normal traction on the surface of the sphere $r=a$. Having the displacement field in terms of the vector spherical harmonics makes it straightforward to apply continuity of the displacement. To apply the traction boundary condition it is necessary to express the traction inside the sphere in terms of the vector spherical harmonics as well

$$\boldsymbol{t}_1^{(r)}(a,\theta,\varphi)=\sum_{\tau\sigma ml} G_{\tau\sigma ml}\boldsymbol{A}_{\tau\sigma ml}(\theta,\varphi), \tag{3.19}$$

where $\boldsymbol{t}_1^{(r)}$ is the traction in the r direction inside the sphere. Here, $G_{\tau\sigma ml}$ has the same coupling among the coefficients $f_{\tau\sigma ml,j}$ as in $H_{\tau\sigma ml}(r)$.

Equations (3.13)–(3.19) give all the necessary relations inside the sphere to apply boundary conditions and solve the scattering problem. Explicit expressions for these equations are not stated here, but it is possible to use such an approach and to solve the scattering problem numerically for low and intermediate frequencies. In the following explicit expressions are provided in the low frequency limit and some numerical calculations are performed for intermediate frequencies.

In the low frequency limit, it is sufficient to expand the displacement field to power 3 in r. Based on equations (3.14)–(3.16), this truncation leads to 64 partial waves for the displacement field inside the sphere which are listed in table 1. The continuity condition of the displacement and traction for each vector spherical harmonic leads to a large system of equations to be solved. Using the already discussed couplings, such a large system of equations is reduced to 12 sets of decoupled systems of equations as listed in table 1. These systems of equations can be reduced more by considering that in the low frequency limit it is sufficient to take only $l=0,1$ and 2. This means that no incident wave of orders $l\geq 3$ needs to be taken into account. Consequently, all partial waves with order $l\geq 3$ inside the sphere (which are mentioned in parentheses in table 1) must vanish due to the displacement continuity condition. In the following sections, the calculation of the **T** matrix elements are discussed for each set of coupling in the low frequency limit.

4. Low frequency T matrix elements for $m = 0$

For the $m = 0$ case the spherical harmonics are φ-independent (see equation (2.5)) and only the even parts ($\sigma = e$) exist. In the low frequency limit, since there is no coupling between $m = 0$, $m = 1$ and $m = 2$, this means that all displacement and traction fields are φ-independent. This means that no coupling occurs between SH waves and P–SV waves and these can be studied separately. In general, however, there is coupling between $m = 0$ and $m = 4$ which leads to φ-dependent fields and coupling between P–SV and SH waves as shown in table 1. The problem can also be decoupled into the even and odd values of l and there exist four decoupled problems, as in table 1, which are studied in the following.

(a) Even–even P–SV waves

First, consider the P–SV case for even values of l. The following ansatz can be made for the displacement field based on equation (3.13)

$$\boldsymbol{u}_1(r,\theta,\varphi) = F_{2e02}(r)\boldsymbol{A}_{2e02}(\theta,\varphi) + F_{3e00}(r)\boldsymbol{A}_{3e00}(\theta,\varphi) + F_{3e02}(r)\boldsymbol{A}_{3e02}(\theta,\varphi), \tag{4.1}$$

where the r-dependent coefficients are expanded into powers of r according to equations (3.15) and (3.16) as

$$\left.\begin{aligned} &F_{2e02}(r) = f_{2e02,1}r + f_{2e02,3}r^3, \quad F_{3e00}(r) = f_{3e00,1}r + f_{3e00,3}r^3 \\ \text{and}\quad &F_{3e02}(r) = f_{3e02,1}r + f_{3e02,3}r^3. \end{aligned}\right\} \tag{4.2}$$

As discussed earlier, in equations (4.1) and (4.2) only terms with power 3 of r and order 2 of l or lower are included since these are sufficient in the low frequency limit, but there is no particular problem in expanding the displacement field to higher orders.

Substituting the expansion of the displacement into the equations of motion and then expanding the equations of motion in terms of the vector spherical harmonics as explained in equation (3.17) lead to the following r-dependent coefficients

$$\left.\begin{aligned} H_{3e00} &= \left(\left(10\alpha_1 + 20\alpha_2 - \frac{9}{2}\beta\right)f_{3e00,3} + \rho_1\omega^2 f_{3e00,1}\right)r^3 = 0, \\ H_{3e02} &= \frac{1}{42}\left(\sqrt{6}f_{2e02,1} - 3f_{3e02,1}\right)(84\alpha_2 - 19\beta)r + \Big(\rho_1\omega^2 f_{3e02,1} \\ &\quad + 2(5\alpha_1 + 7\alpha_2 + 3\beta)f_{3e02,3} + \sqrt{\frac{2}{3}}(-4\alpha_1 + 7\beta)f_{2e02,3}\Big)r^3 = 0 \\ \text{and}\quad H_{2e02} &= \frac{-1}{3}\left(2f_{2e02,1} - \sqrt{6}f_{3e02,1}\right)(9\alpha_1 + 15\alpha_2 - 2\beta)r + \Big(\rho_1\omega^2 f_{2e02,1} \\ &\quad + \sqrt{6}(5\alpha_1 + 7\alpha_2 + 3\beta)f_{3e02,3} + \left(-6\alpha_1 + \frac{21}{2}\beta\right)f_{2e02,3}\Big)r^3 = 0. \end{aligned}\right\} \tag{4.3}$$

These coefficients are the only ones that only contain the $f_{\tau\sigma ml}$ explicitly shown in equation (4.2). The linear independence of the powers of r gives the recursion relations among the expansion coefficients

$$\left.\begin{aligned} &f_{2e02,1} = \sqrt{\frac{3}{2}}f_{3e02,1}, \quad f_{3e00,3} = \frac{-2}{(20\alpha_1 + 40\alpha_2 - 9\beta)}\rho_1\omega^2 f_{3e00,1} \\ \text{and}\quad &f_{2e02,3} = \frac{\sqrt{2}}{\sqrt{3}(4\alpha_1 - 7\beta)}(2(5\alpha_1 + 7\alpha_2 + 3\beta)f_{3e02,3} + \rho_1\omega^2 f_{3e02,1}). \end{aligned}\right\} \tag{4.4}$$

It can be observed that there is no coupling between the $l = 0$ and $l = 2$ coefficients. This is an exception for $l = 0$ and $l = 2$, while for higher values of l there is coupling between l and $l \pm 2$. These recursion relations reduce the number of coefficients inside the sphere for this case to three. In general, only one unknown coefficient remains for each vector spherical harmonics inside the sphere. Besides the displacement ansatz expressed in equation (4.1) the traction expansion can

also be derived according to equation (3.19); however, these are large expressions and are not presented.

In the surrounding medium, the expansion coefficients of the scattered wave for even–even P–SV waves are h_{2e02}, h_{3e00} and h_{3e02} and the unknowns inside the sphere are $f_{3e00,1}$, $f_{3e02,1}$, $f_{3e02,3}$. These six unknown coefficients are found by applying continuity of the displacement and traction for $\tau = 2$ with $l = 2$ and $\tau = 3$ with $l = 0, 2$. This leads to a system of six equations in six unknowns and an expansion in the sphere radius a then leads to the following dominating **T** matrix elements for low frequencies

$$\left.\begin{aligned} T_{3e00,3e00} &= -\mathrm{i}(k_p a)^3 \left(\frac{1}{3} - \frac{\lambda + 2\mu}{C_{11} + 2C_{12} + 4\mu}\right), \\ T_{2e02,2e02} &= -\mathrm{i}(k_s a)^3 \frac{(\lambda + 2\mu)(C_{11} - C_{12} - 2\mu)}{2\mu(4C_{11} - 4C_{12} + 7\mu) + 3\lambda(C_{11} - C_{12} + 3\mu)}, \\ T_{3e02,2e02} &= T_{2e02,3e02} = -\mathrm{i}\sqrt{\frac{2k_p}{3k_s}}(k_s a)^3 \frac{\mu(C_{11} - C_{12} - 2\mu)}{2\mu(4C_{11} - 4C_{12} + 7\mu) + 3\lambda(C_{11} - C_{12} + 3\mu)} \\ \text{and} \quad T_{3e02,3e02} &= -\mathrm{i}\frac{2}{3}(k_p a)^3 \frac{\mu(C_{11} - C_{12} - 2\mu)}{2\mu(4C_{11} - 4C_{12} + 7\mu) + 3\lambda(C_{11} - C_{12} + 3\mu)}. \end{aligned}\right\} \tag{4.5}$$

Since there is no coupling between $l = 0$ and $l = 2$ for $m = 0$, the following **T** matrix elements are zero for low frequencies

$$T_{2e02,3e00} = T_{3e00,2e02} = T_{3e02,3e00} = T_{3e00,3e02} = 0. \tag{4.6}$$

In the isotropic limit when $C_{44} = (C_{11} - C_{12})/2$, the **T** matrix elements become the same as those of the isotropic case (given by Boström [35]).

(b) Even–odd P–SV waves

For the case with odd values of l for P–SV waves, the low frequency displacement field expansion is

$$\boldsymbol{u}_1(r, \theta, \varphi) = F_{2e01}(r)\boldsymbol{A}_{2e01}(\theta, \varphi) + F_{3e01}(r)\boldsymbol{A}_{3e01}(\theta, \varphi), \tag{4.7}$$

where

$$F_{2e01}(r) = f_{2e01,0} + f_{2e01,2}r^2 \quad \text{and} \quad F_{3e01}(r) = f_{3e01,0} + f_{3e01,2}r^2. \tag{4.8}$$

As in the previous subsection the equations of motion lead to the following recursion relations

$$f_{2e01,0} = \sqrt{2} f_{3e01,0} \quad \text{and} \quad f_{2e01,2} = \frac{(8\alpha_1 + 12\alpha_2 - 3\beta) f_{3e01,2} + 2\rho_1 \omega^2 f_{3e01,0}}{2\sqrt{2}(\alpha_1 - \alpha_2)}. \tag{4.9}$$

Thus, two unknowns remain inside the sphere and the unknowns outside the sphere are h_{2e01} and h_{3e01}. These are found by considering continuity of the displacement and traction for $\tau = 2$ and $\tau = 3$ with $l = 1$, and the **T** matrix elements are derived as

$$\left.\begin{aligned} T_{2e01,2e01} &= -\frac{2}{9}\mathrm{i}(k_s a)^3 \left(1 - \frac{\rho_1}{\rho}\right), \\ T_{3e01,2e01} &= T_{2e01,3e01} = -\frac{\sqrt{2}}{9}\mathrm{i}\sqrt{k_p^3 k_s^3}\, a^3 \left(1 - \frac{\rho_1}{\rho}\right) \\ \text{and} \quad T_{3e01,3e01} &= -\frac{1}{9}\mathrm{i}(k_p a)^3 \left(1 - \frac{\rho_1}{\rho}\right). \end{aligned}\right\} \tag{4.10}$$

It can be observed that the **T** matrix elements only depend on the density of the sphere and not its elastic properties. This is reasonable since the $l = 1$ case for low frequencies is related to the rigid body translation. Since the stiffness constants of the sphere are not important, these elements are the same for any type of spherical inclusion.

(c) Even–odd SH waves

The first possible order for the even SH waves with $m=0$ is $l=1$, and the displacement field expansion for this case is

$$\boldsymbol{u}_1(r,\theta,\varphi)=F_{1e01}(r)\boldsymbol{A}_{1e01}(\theta,\varphi). \tag{4.11}$$

The r-dependent coefficient is expanded into powers of r based on equation (3.14) as

$$F_{1e01}(r)=f_{1e01,1}r+f_{1e01,3}r^3. \tag{4.12}$$

The governing equation inside the sphere yields

$$f_{1e01,3}=\frac{2\rho_1\omega^2}{20\alpha_2-3\beta}f_{1e01,1}. \tag{4.13}$$

Therefore, only one unknown remains inside the sphere which together with the expansion coefficient of the scattered wave for $m=0$, $l=1$ (h_{1e01}) give two unknowns. Using the continuity of the displacement and traction for $\tau=1$ $l=1$, the following $\mathbf{T}$ matrix element is derived

$$T_{1e01,1e01}=-\frac{1}{45}\mathrm{i}(k_sa)^5\left(1-\frac{\rho_1}{\rho}\right). \tag{4.14}$$

This element depends only on the density of the sphere and corresponds to a rigid body rotation of the sphere at low frequencies due to an incident torsional wave. As seen this element has leading order $(ka)^5$. Other $\mathbf{T}$ matrix elements involving SH waves (including even–even SH waves for the $m=0$ case) have the same leading order ($(ka)^5$) which is higher than the leading order of the P–SV case ($(ka)^3$) and thus are not presented here.

5. Low frequency T matrix elements for $m=1$

For the $m=1$ case, waves may be even or odd with respect to φ (σ values) and as discussed in §3 the P–SV and SH waves are coupled with different parities. The problem can still be decoupled for even and odd values of σ and l. This means that there are four decoupled problems, even–even, even–odd, odd–even and odd–odd. In the $m=1$ case, different parity with respect to φ means choosing between $\cos\varphi$ and $\sin\varphi$, but this corresponds to a rotation by $\pi/2$ around the z axis and as the cubic material is unaffected by such a rotation the $\mathbf{T}$ matrix elements should be the same for the even and odd cases. Thus, even–even and odd–even cases are identical as well as even–odd and odd–odd cases. This means that it is enough to study two decoupled problems.

(a) Even–even P–SV waves and odd–odd SH waves

First the even–even case is studied. The even–even P–SV waves are coupled with the odd–odd SH waves and the ansatz for the displacement is

$$\boldsymbol{u}_1(r,\theta,\varphi)=F_{1o11}(r)\boldsymbol{A}_{1o11}(\theta,\varphi)+F_{2e12}(r)\boldsymbol{A}_{2e12}(\theta,\varphi)+F_{3e12}(r)\boldsymbol{A}_{3e12}(\theta,\varphi), \tag{5.1}$$

where $F_{1o13}(r)$, $F_{1o33}(r)$, $F_{2e14}(r)$ and $F_{3e14}(r)$ are considered to be zero since there are no incoming waves of order $l>2$. The r-dependent coefficients are expanded to power 3 in r as

$$\left.\begin{aligned}F_{1o11}(r)&=f_{1o11,1}r+f_{1o11,3}r^3,\\ F_{2e12}(r)&=f_{2e12,1}r+f_{2e12,3}r^3\end{aligned}\right\} \tag{5.2}$$

and

$$F_{3e12}(r)=f_{3e12,1}r+f_{3e12,3}r^3.$$

Using the equations of motion the relations among these unknown coefficients become

$$\left.\begin{aligned} f_{1o11,1} &= \frac{-1}{2\rho_1\omega^2}(20\alpha_2 - 3\beta)f_{1o11,3}, \quad f_{2e12,1} = \sqrt{\frac{3}{2}}f_{3e12,1} \\ \text{and} \quad f_{2e12,3} &= \frac{\sqrt{6}}{12\alpha_1 + 11\beta}\left(2(5\alpha_1 + 7\alpha_2 - 5\beta)f_{3e12,3} + \sqrt{6}\rho_1\omega f_{3e12,1}\right). \end{aligned}\right\} \tag{5.3}$$

The SH waves coefficients are independent of the ones for P–SV waves which is a special case happening only for the lowest order. This means that the P–SV waves and SH waves are decoupled for the leading order **T** matrix elements and thus can be studied separately. Knowing that the **T** matrix elements of the SH case are of higher order in comparison with the P–SV case, only the **T** matrix elements of the P–SV waves are derived. After applying the boundary conditions these become

$$\left.\begin{aligned} T_{2\sigma 12,2\sigma 12} &= -\mathrm{i}(k_s a)^3 \frac{(\lambda + 2\mu)(2C_{44} - 2\mu)}{2\mu(8C_{44} + 7\mu) + 3\lambda(2C_{44} + 3\mu)}, \\ T_{3\sigma 12,2\sigma 12} &= T_{2\sigma 12,3\sigma 12} = -\mathrm{i}\sqrt{\frac{2k_p}{3k_s}}(k_s a)^3 \frac{\mu(2C_{44} - 2\mu)}{2\mu(8C_{44} + 7\mu) + 3\lambda(2C_{44} + 3\mu)} \\ \text{and} \quad T_{3\sigma 12,3\sigma 12} &= -\mathrm{i}\frac{2}{3}(k_p a)^3 \frac{\mu(2C_{44} - 2\mu)}{2\mu(8C_{44} + 7\mu) + 3\lambda(2C_{44} + 3\mu)}, \end{aligned}\right\} \tag{5.4}$$

where σ may be e (even) or o (odd) as the **T** matrix elements are the same for these two cases. Of course, these elements of the **T** matrix are also the same as in the isotropic case in the isotropic limit.

(b) Odd–odd P–SV waves even–even SH waves

The odd–odd P–SV waves which are coupled with even–even SH waves are next studied. Truncating the displacement ansatz in the same manner as in the previous sections, the appropriate displacement expansion is

$$\mathbf{u}(r,\theta,\varphi) = F_{1e12}(r)\boldsymbol{A}_{1e12}(\theta,\varphi) + F_{2o11}(r)\boldsymbol{A}_{2o11}(\theta,\varphi) + F_{3o11}(r)\boldsymbol{A}_{3o11}(\theta,\varphi), \tag{5.5}$$

where

$$\left.\begin{aligned} F_{1e12}(r) &= f_{1e12,2}r^2, \\ F_{2o11}(r) &= f_{2o11,0} + f_{2o11,2}r^2 \\ \text{and} \quad F_{3o11}(r) &= f_{3o11,0} + f_{3o11,2}r^2. \end{aligned}\right\} \tag{5.6}$$

Using the equations of motion the recursion relations among the unknown coefficients are obtained as

$$\left.\begin{aligned} f_{2o11,0} &= \sqrt{2}f_{3o11,0} \\ \text{and} \quad f_{2o11,2} &= \frac{1}{2\sqrt{2}(\alpha_1 - \alpha_2)}((8\alpha_1 + 12\alpha_2 - 3\beta)f_{3o11,2} + 2\rho_1\omega^2 f_{3o11,0}), \end{aligned}\right\} \tag{5.7}$$

where there is no coupling between P–SV and SH waves to lowest order. The **T** matrix elements for the P–SV waves become

$$\left.\begin{aligned} T_{2\sigma 11,2\sigma 11} &= -\frac{2}{9}\mathrm{i}(k_s a)^3\left(1 - \frac{\rho_1}{\rho}\right), \\ T_{3\sigma 11,2\sigma 11} &= T_{2\sigma 11,3\sigma 11} = -\frac{\sqrt{2}}{9}\mathrm{i}\sqrt{k_p^3 k_s^3}a^3\left(1 - \frac{\rho_1}{\rho}\right) \\ \text{and} \quad T_{3\sigma 11,3\sigma 11} &= -\frac{1}{9}\mathrm{i}(k_p a)^3\left(1 - \frac{\rho_1}{\rho}\right). \end{aligned}\right\} \tag{5.8}$$

Here again $\sigma = e$ or o. As is to be expected these elements only depend on the density of the sphere since $l = 1$ for low frequencies corresponds to rigid body translation. In fact these elements are the same as the **T** matrix elements for $m = 0$ and $l = 1$ given in equations (4.10) and (5.8).

6. Low frequency T matrix elements for $m = 2$

For the $m = 2$ case, the problem can be decoupled in the same way as in §5 for $m = 1$, which means there are four decoupled problems with even–even, even–odd, odd–even and odd–odd parities of the P–SV waves. However, the even and odd cases with respect to φ may differ. By considering the condition $l \geq m$ for the vector spherical harmonics, the only necessary l value for the low frequency study is $l = 2$. Therefore, it is sufficient to consider only even waves with respect to θ which means P–SV waves with $l = 2$, and SH waves with $l = 2$ without any coupling. Considering the fact that the **T** matrix elements for the SH waves are of order $(k_s a)^5$ or higher only the P–SV waves are studied here. The P–SV waves for $l = 2$ may be even or odd with respect to φ and these two cases are sufficient for the leading order **T** matrix elements of this study.

(a) Even–even P–SV waves

The displacement ansatz for the even–even P–SV waves can be truncated for low frequencies as

$$\boldsymbol{u}_1(r,\theta,\varphi) = F_{2e22}(r)\boldsymbol{A}_{2e22}(\theta,\varphi) + F_{3e22}(r)\boldsymbol{A}_{3e22}(\theta,\varphi), \tag{6.1}$$

where

$$\left.\begin{aligned} F_{2e22}(r) &= f_{2e22,1}r + f_{2e22,3}r^3 \\ \text{and} \quad F_{3e22}(r) &= f_{3e22,1}r + f_{3e22,3}r^3. \end{aligned}\right\} \tag{6.2}$$

The recurrence relations follow in the usual way

$$\left.\begin{aligned} f_{2e22,1} &= \sqrt{\frac{3}{2}} f_{3e22,1} \\ \text{and} \quad f_{2e22,3} &= \frac{\sqrt{2}}{\sqrt{3}(4\alpha_1 - 7\beta)}(2(5\alpha_1 + 7\alpha_2 + 3\beta)f_{3e22,3} + \rho_1\omega^2 f_{3e22,1}). \end{aligned}\right\} \tag{6.3}$$

Finally, applying continuity of the displacement and traction for $l = 2$, $\tau = 2$ and $\tau = 3$, the following **T** matrix elements are derived

$$\left.\begin{aligned} T_{2e22,2e22} &= -\mathrm{i}(k_s a)^3 \frac{(\lambda + 2\mu)(C_{11} - C_{12} - 2\mu)}{2\mu(4C_{11} - 4C_{12} + 7\mu) + 3\lambda(C_{11} - C_{12} + 3\mu)}, \\ T_{3e22,2e22} &= T_{2e22,3e22} = -\mathrm{i}\sqrt{\frac{2k_p}{3k_s}}(k_s a)^3 \frac{\mu(C_{11} - C_{12} - 2\mu)}{2\mu(4C_{11} - 4C_{12} + 7\mu) + 3\lambda(C_{11} - C_{12} + 3\mu)} \\ \text{and} \quad T_{3e22,3e22} &= -\mathrm{i}\frac{2}{3}(k_p a)^3 \frac{\mu(C_{11} - C_{12} - 2\mu)}{2\mu(4C_{11} - 4C_{12} + 7\mu) + 3\lambda(C_{11} - C_{12} + 3\mu)}. \end{aligned}\right\} \tag{6.4}$$

These **T** matrix elements are identical with those for $m = 0$.

(b) Odd–even P–SV waves

Similarly, the displacement ansatz for the odd–even P–SV waves for low frequencies is

$$\boldsymbol{u}_1(r,\theta,\varphi) = F_{2o22}(r)\boldsymbol{A}_{2o22}(\theta,\varphi) + F_{3o22}(r)\boldsymbol{A}_{3o22}(\theta,\varphi), \tag{6.5}$$

where

$$\left.\begin{aligned} F_{2o22}(r) &= f_{2o22,1}r + f_{2o22,3}r^3 \\ \text{and} \quad F_{3o22}(r) &= f_{3o22,1}r + f_{3o22,3}r^3. \end{aligned}\right\} \tag{6.6}$$

For these coefficients the recursion relations become

$$f_{2o22,1} = \sqrt{\frac{3}{2}} f_{3o22,1}$$

and

$$f_{2o22,3} = \frac{\sqrt{6}}{(12\alpha_1 + 11\beta)} (2(5\alpha_1 + 7\alpha_2 - 5\beta) f_{3o22,3} + \rho_1 \omega^2 f_{3o22,1}). \tag{6.7}$$

Finally, applying the boundary conditions, the following **T** matrix elements are derived

$$T_{2o22,2o22} = -\mathrm{i}(k_s a)^3 \frac{(\lambda + 2\mu)(2C_{44} - 2\mu)}{2\mu(8C_{44} + 7\mu) + 3\lambda(2C_{44} + 3\mu)},$$

$$T_{3o22,2o22} = T_{2o22,3o22} = -\mathrm{i}\sqrt{\frac{2k_p}{3k_s}} (k_s a)^3 \frac{\mu(2C_{44} - 2\mu)}{2\mu(8C_{44} + 7\mu) + 3\lambda(2C_{44} + 3\mu)} \tag{6.8}$$

and

$$T_{3o22,3o22} = -\mathrm{i}\frac{2}{3} (k_p a)^3 \frac{\mu(2C_{44} - 2\mu)}{2\mu(8C_{44} + 7\mu) + 3\lambda(2C_{44} + 3\mu)},$$

which are the same as the **T** matrix elements for $m = 1$.

7. Polycrystalline materials

In this section, wave propagation in single phase polycrystalline materials is studied. The grains are equiaxed, anisotropic and randomly oriented which make the polycrystalline material macroscopically isotropic and homogeneous [22]. In these materials, the geometry of the grains can be modelled in various ways, in a stochastic way or as individual grains. Here the stochastic approach, which is followed in much of the literature, is reviewed briefly. On the other hand, the present approach follows the individual grain perspective, specifically for the low frequency limit. Thus, the effective wave numbers are derived based on single grain **T** matrix elements studied in §§4–6.

Stochastic models treat the medium as a whole in terms of the geometric statistics of the grains which directly reflect the macroscopic properties of the polycrystalline material [22]. In these models, the elastic medium is described by a local elastic stiffness tensor which is a random function of the spatial coordinates. The fluctuations with respect to the mean elastic tensor (normally the Voigt average) are considered to be small and described by a TPC function, giving the probability of two points lying in the same grain. The TPC function can also be defined in a way to capture various volume distributions of grains or even non-equiaxed grains. These models are accurate when the second order degree of inhomogeneity is small and hence are called the second order approximation (SOA). With such a definition of the medium, the elastodynamic equations governing the polycrystalline material are a system of partial differential equations with random coefficients which is not solvable in general. Instead, the mean perturbed field is studied using volume integral equations and some perturbation methods. The SOA model involves Cauchy integral equations which need to be solved numerically. The FFA, introduced by Rokhlin *et al.* [24], can be made to eliminate the complex calculation of the Cauchy integrals. These methods (SOA and FFA) normally do not lead to a closed form solution for the perturbed wave number K unless by considering more assumptions like the Rayleigh asymptote (valid for low frequencies), or the stochastic asymptote (valid for high frequencies). Closed form solutions of the effective wavenumber valid for all frequencies are also derived by invoking the Born approximation for the SOA and FFA models [24,32,34]. An overview of these models with a comparison of the various approximations is covered by Sha *et al.* [32]. Since the calculations of the present approach are carried out in the low frequency range, the closed form expressions of the attenuation and phase velocity (which are the imaginary and real part of the complex effective

wave number, respectively) with the Rayleigh asymptote in polycrystalline materials with cubic symmetry calculated by Sha *et al.* [32] are expressed here for comparison purposes

$$\left.\begin{aligned}\alpha_p &= \frac{128\pi^3\beta^2 f^4 V}{\rho^2 c_p^3}\left(\frac{\Delta_1}{c_p^5}+\frac{\Delta_2}{c_s^5}\right), \quad \frac{c_p}{C_p} = 1+2\left(\frac{4\beta}{\rho c_p}\right)^2\left(\frac{\Delta_1}{c_p^2}+\frac{\Delta_2}{c_s^2}\right)\\ \text{and}\qquad \alpha_s &= \frac{128\pi^3\beta^2 f^4 V}{\rho^2 c_s^3}\left(\frac{\Delta_3}{c_p^5}+\frac{\Delta_4}{c_s^5}\right), \quad \frac{c_s}{C_s} = 1+2\left(\frac{4\beta}{\rho c_s}\right)^2\left(\frac{\Delta_3}{c_p^2}+\frac{\Delta_4}{c_s^2}\right).\end{aligned}\right\} \tag{7.1}$$

Here, α_p and α_s are longitudinal and transverse attenuation coefficients, respectively, c_p and c_s are the unperturbed medium longitudinal and transverse wave velocities, respectively, C_p and C_s are the effective longitudinal and transverse wave velocities, respectively, V is the effective grain volume calculated based on the TPC function, and $\Delta_1 = 8/375$, $\Delta_2 = 4/125$, $\Delta_3 = 2/125$ and $\Delta_4 = 3/125$.

In the present approach, a polycrystalline material is viewed as a special case of a distribution of inclusions. Accordingly, the scattering by each grain of the polycrystal is regarded as taking place in the effective, homogeneous and isotropic medium of all the other grains (ignoring attenuation in the material). An approach to study the effective wavenumber in materials with a distribution of inclusions is developed by Foldy [17], where each inclusion is treated as if it were a single scatterer in the unperturbed medium. The wavenumber of the perturbed medium is related to the scattering coefficient of each inclusion together with the wave number of the unperturbed medium (matrix) and the distribution of the inclusions. The effective wave number of the perturbed medium is thus derived as [19]

$$K_i^2 = k_i^2 + 4\pi N \bar{f}_i, \tag{7.2}$$

where the index i can be p or s for longitudinal and transverse waves, respectively, k_i is the wave number of the matrix, N is the number density of inclusions, $\bar{f}_i$ is the average (over all orientations of the grains) forward scattering amplitude. Foldy theory is valid for dilute concentration of inclusions, typically $d < 0.05$, where d is the relative density of the grains.

In the present approach, the grains in the polycrystalline material are considered to be spheres with the same radius a. This is a reasonable approximation for low frequencies, for which the scattering is mainly a volume effect. As crystals in a polycrystalline material fill the volume, the number density of inclusions can be put to $d = 1$, meaning that the spheres must be partially overlapping. Although this high density of inclusions violates the bound that is usually expected for the Foldy approach, this should be reasonable as the scattering by each sphere is extremely small, and consequently multiple scattering is even smaller and can be neglected. Therefore, the average forward scattering amplitudes in terms of the **T** matrix elements calculated in previous sections are [21]

$$\left.\begin{aligned}\bar{f}_p &= -\frac{i}{k_p}\sum_{\sigma ml} T_{3\sigma ml,3\sigma ml}\\ \text{and}\qquad \bar{f}_s &= -\frac{i}{2k_s}\sum_{\substack{\tau\sigma ml\\ \tau=1,2}} T_{\tau\sigma ml,\tau\sigma ml}.\end{aligned}\right\} \tag{7.3}$$

The effective wave numbers then become

$$\left.\begin{aligned}\left(\frac{K_p}{k_p}\right)^2 &= 1-\frac{4\pi i d}{V k_p^3}\sum_{\sigma ml} T_{3\sigma ml,3\sigma ml}\\ \text{and}\qquad \left(\frac{K_s}{k_s}\right)^2 &= 1-\frac{2\pi i d}{V k_s^3}\sum_{\substack{\tau\sigma ml\\ \tau=1,2}} T_{\tau\sigma ml,\tau\sigma ml},\end{aligned}\right\} \tag{7.4}$$

where $V = 4\pi a^3/3$ is the volume of a single grain and K_i, $i = p, s$ are the polycrystalline effective wave numbers. The resulting complex effective wave number describes the attenuation and phase

velocity of the composite medium as

$$\left.\begin{aligned}\frac{\alpha_i}{k_i} &= \mathrm{Im}\,\frac{K_i}{k_i}\\ \text{and}\qquad \frac{C_i}{c_i} &= \mathrm{Re}\,\frac{k_i}{K_i},\end{aligned}\right\} \tag{7.5}$$

where α_i is the attenuation, c_i is the phase velocity in the matrix and C_i is the effective phase velocity.

Looking at the **T** matrix elements calculated in §§4–6, the leading order in the low frequency limit are all imaginary which leads to a real effective wavenumber. To obtain attenuation, the leading order real parts of the **T** matrix elements are also needed. Using the 'Hermitian' property of the **T** matrix [36]

$$\mathbf{T}^{\dagger}\mathbf{T} = -\mathrm{Re}\mathbf{T}, \tag{7.6}$$

the leading order real parts of **T** matrix elements are obtained.

Collecting everything, the leading order real and imaginary parts of the effective wave numbers K_i become

$$\left.\begin{aligned}\left(\frac{K_p}{k_p}\right)^2 &= 1 + A_p + B_p i\\ \text{and}\qquad \left(\frac{K_s}{k_s}\right)^2 &= 1 + A_s + B_s i,\end{aligned}\right\} \tag{7.7}$$

where the coefficients are real and given by

$$\left.\begin{aligned}
A_p &= \frac{3(\lambda+2\mu)}{C_{11}+2C_{12}+4\mu} - \frac{6\mu(2C_{44}-2\mu)}{2\mu(8C_{44}+7\mu)+3\lambda(2C_{44}+3\mu)}\\
&\quad - \frac{4\mu(C_{11}-C_{12}-2\mu)}{2\mu(4C_{11}-4C_{12}+7\mu)+3\lambda(C_{11}-C_{12}+3\mu)} + \frac{\rho_1-\rho}{\rho} - 1,\\
B_p &= \frac{(k_p a)^3}{9}\left[3\left(\frac{3(\lambda+2\mu)}{C_{11}+2C_{12}+4\mu}-1\right)^2 + \left(1+2\frac{k_s^3}{k_p^3}\right)\left(\frac{\rho_1-\rho}{\rho}\right)^2\right.\\
&\quad + 18\left(2+3\frac{k_s^5}{k_p^5}\right)\left(\frac{\mu(2C_{44}-2\mu)}{2\mu(8C_{44}+7\mu)+3\lambda(2C_{44}+3\mu)}\right)^2\\
&\quad \left.+ 12\left(2+3\frac{k_s^5}{k_p^5}\right)\left(\frac{\mu(C_{11}-C_{12}-2\mu)}{2\mu(4C_{11}-4C_{12}+7\mu)+3\lambda(C_{11}-C_{12}+3\mu)}\right)^2\right],\\
A_s &= -\frac{9(\lambda+2\mu)(2C_{44}-2\mu)}{4\mu(8C_{44}+7\mu)+6\lambda(2C_{44}+3\mu)}\\
&\quad - \frac{3(\lambda+2\mu)(C_{11}-C_{12}-2\mu)}{2\mu(4C_{11}-4C_{12}+7\mu)+3\lambda(C_{11}-C_{12}+3\mu)} + \frac{\rho_1-\rho}{\rho}\\
\text{and}\qquad B_s &= \frac{(k_s a)^3}{9}\left[\frac{27}{2}\left(3+2\frac{k_p^5}{k_s^5}\right)\left(\frac{(\lambda+2\mu)(2C_{44}-2\mu)}{2\mu(8C_{44}+7\mu)+3\lambda(2C_{44}+3\mu)}\right)^2\right.\\
&\quad + 9\left(3+2\frac{k_p^5}{k_s^5}\right)\left(\frac{(\lambda+2\mu)(C_{11}-C_{12}-2\mu)}{2\mu(4C_{11}-4C_{12}+7\mu)+3\lambda(C_{11}-C_{12}+3\mu)}\right)^2\\
&\quad \left.+ \left(2+\frac{k_p^3}{k_s^3}\right)\left(\frac{\rho_1-\rho}{\rho}\right)^2.\right.
\end{aligned}\right\} \tag{7.8}$$

Since in the low frequency limit the parameters A_i and B_i are small, the normalized attenuation and phase velocity can be approximated with good accuracy as

$$\left.\begin{aligned}\frac{\alpha_i}{k_i} &= \frac{B_i}{2}\\ \text{and}\qquad \frac{c_i}{C_i} &= 1+\frac{A_i}{2}.\end{aligned}\right\} \tag{7.9}$$

These relations confirm the frequency dependence of attenuation and phase velocity at low frequencies where the phase velocity is independent of frequency and the attenuation depends on the fourth power of the frequency (or wavenumber).

8. Numerical results for polycrystalline materials

In this section, some numerical results are given for polycrystalline materials with cubic symmetry. To verify the present approach and to highlight its strengths and limitations, the results are compared with the closed form expressions of the effective wave numbers using the Born approximation of the FFA model (as expressed in [34]) and the Rayleigh asymptote of the SOA method for low frequencies (as in equation (7.1) [32]). These are also compared with the numerical calculations of the SOA and FEMs presented by Huang *et al.* [34]. To compare the analytical methods with FEM, a suitable adaptation of the geometrical model considered in the analytical methods with the one developed in the FEM model is necessary.

As in the analytical methods, single phase polycrystals with randomly oriented crystallographic axes are considered in FEM [30]. The methodology of FEM is described in detail by Van Pamel *et al.* [30], where different aspects regarding background theory, medium generation, FE spatial discretization, material model, loading and boundary conditions for the FEM are addressed. The adaptation of the stochastic models (SOA and Born) with the model developed in FEM can be done by a suitable definition of the TPC function. An appropriate TPC function according to the geometrical model generated by Van Pamel *et al.* [29] for FE calculations is defined by Sha *et al.* [32] and is called the generalized TPC function (as opposed to the exponential TPC function initially used in the literature).

On the other hand, the geometrical model in the present method is spherical grains with the same radius a. In the low frequency range, which is the target range of the present approach, the important geometrical property of the grains, which determines the scattering, is the average grain volume. Thus, a proper adaptation is having the same average grain volume ($V = 4\pi a^3/3$) in the present approach with the effective grain volume of the stochastic models derived based on the generalized TPC function. For the generalized TPC function, based on the FEM grain size distribution [32], the effective grain volume in the SOA method is $V = 0.1459\,\text{mm}^3$, thus the radius of the grains in the present model is chosen as $a = 0.3266\,\text{mm}$ which is used as the normalization radius in the following calculations.

Another important aspect in the analytical calculations of the polycrystalline materials' effective wave numbers (K_p and K_s) is the material properties of the macroscopically homogeneous and isotropic material. This is the surrounding isotropic medium of each grain in the present approach and the unperturbed medium in the stochastic models (for brevity in the following it is called the matrix properties). In the single phase polycrystalline medium, the density is the same everywhere and the matrix has the same density as each grain, thus $\rho = \rho_1$. Then some terms in the explicit expressions of the present method giving the attenuation and phase velocity (equation (7.9)) vanish. The other matrix properties can be given by the longitudinal and transverse wave numbers (k_p and k_s). It is customary in this context to use the Voigt average as an approximation of the matrix properties and calculate the matrix wave numbers as $k_p^2 = \rho\omega^2/(\lambda + 2\mu)$ and $k_s^2 = \rho\omega^2/\mu$, where the Voigt average of the Lamé constants for

Table 2. Table of materials properties [34].

material properties									
	stiffness constants (Gpa)			density (g cm^{-3})	anisotropy factor	Voigt average (Gpa)		present average (Gpa)	
	C_{11}	C_{12}	C_{44}	ρ	A	λ	μ	λ	μ
Al	103.4	57.10	28.60	2700	1.24	54.92	26.42	55.00	26.29
In	234.6	145.4	126.2	8260	2.83	112.8	93.56	119.1	84.11
Cu	169.6	122.4	74.00	8935	3.14	102.2	53.84	106.3	47.68
Li	13.40	11.30	9.600	534.0	9.14	7.880	6.180	9.118	4.322

materials with cubic symmetry are

$$\left.\begin{aligned}\lambda &= \frac{1}{5}(C_{11} + 4C_{12} - 2C_{44})\\ \text{and}\qquad \mu &= \frac{1}{5}(C_{11} - C_{12} + 3C_{44}).\end{aligned}\right\} \tag{8.1}$$

It is noted that this estimation can be improved by taking an iterative procedure and consider the calculated effective wavenumber (K_i) as the wave number of the matrix (k_i) and iterate the calculations. Of course, since the effective wave number is a complex number with frequency dependence, the iterated calculations are more complicated. This complication can be avoided by considering only the real part of the effective wavenumber at low frequencies. Here this is called the effective quasi-static phase velocity (C_i^{q-s}) and is given in equation (7.9) for the present method. The phase velocity c_i of the matrix can be estimated by putting $c_i = C_i^{q-s}$ which gives $A_i = 0$ (see equation (7.9)). Simplifying $A_i = 0$ leads to the following two relations among the average Lamé constants

$$\lambda = \frac{1}{12}(12\alpha_1 + 8\alpha_2 - 3\beta - 8\mu), \tag{8.2}$$

where μ is the positive real root of the following polynomial of order 3

$$\begin{aligned}&(4\alpha_2 - 7\beta)(12\alpha_1 + 8\alpha_2 - 3\beta)(4\alpha_2 + 9\beta) + 2(4\alpha_2 - 7\beta)(12\alpha_1 + 56\alpha_2 + 105\beta)\mu\\ &\quad - 8(36\alpha_1 + 40\alpha_2 + 27\beta)\mu^2 - 256\mu^3 = 0.\end{aligned} \tag{8.3}$$

Such a procedure for estimating matrix properties is not applicable in the SOA methods since the normalized phase velocity C_p/c_p is an increasing function of the phase velocities c_p and c_s of the matrix with an upper limit of one (equations (7.1)). Thus, the effective quasi-static phase velocity in the SOA method always becomes smaller than any estimated phase velocity of the matrix.

In the following, the attenuation and phase velocity are calculated with both the Voigt and present averages for four different materials with cubic symmetry and different degrees of anisotropy. The degree of anisotropy is measured by the Zener anisotropy index

$$A = \frac{2C_{44}}{C_{11} - C_{12}}. \tag{8.4}$$

A material has a higher degree of anisotropy as A increases and in the case of isotropy $A = 1$. Table 2 shows the elasticity properties and anisotropy indices together with the Voigt and present averages of the Lamé constants of aluminium, inconel, copper and lithium as given by Huang *et al.* [34].

Longitudinal attenuation and phase velocity for these materials are computed using the present, SOA and Born approximation of the FFA methods and are compared with FEM. Calculations for the present method are performed using equations (7.5) and (7.4), first with the explicit expressions of the **T** matrix elements in low frequency limit (which is referred to as the

Rayleigh asymptote of the present method (R–P)), then with the numerical computations carried out with truncations at $l_{\max} = m_{\max} = 6$, and $j_{\max} = 7$ (referred as N–P). For the SOA method both the explicit expression using the Rayleigh asymptote expressed in equation (7.1) (referred to as R–SOA) and numerical calculations for all the frequency range evaluated by Huang *et al.* [34] using the generalized TPC function (referred as SOA) are considered. For the Born approximation of the FFA method, the explicit expressions expressed in [24,32,34] are used (referred as Born). In these methods, both the Voigt and present averages for the matrix properties are studied (except for the SOA method since the numerical results are only available for the Voigt average). Finally, these results are compared with the results of FEM presented by Huang *et al.* [34]

Figure 2 shows (*a*) normalized longitudinal phase velocity C_p/c_p and (*b*) normalized longitudinal attenuation $\alpha_p a$ versus normalized frequency $k_p a$ in the four cubic polycrystals with anisotropy factors $A > 1$ and the Voigt average for the matrix properties as stated in table 2. For each material, the phase velocity and attenuation are calculated with the R–P method (dashed black lines), the N–P method (solid bule lines), the R–SOA method (dash-dotted black lines), the SOA method (solid red lines), and the Born method (dashed green lines) and compared with the FEM results (solid black lines). The quasi-static phase velocities of the FE calculations are also depicted with solid black points in the leftmost of figure 2*a*. Correspondence of these methods with FEM in the calculation of the attenuation is then quantified by defining the error as $(|\alpha - \alpha_{\text{FEM}}|/\alpha_{\text{FEM}})$ in percent, and showing it versus normalized frequency $k_p a$ in figure 2*c*. The FEM results are of course not exact, both because of modelling issues (size of sample, generation of grains) and numerical issues (discretization errors, etc.). An indication of the inaccuracies in the FEM results are given by the fact that the FE curves in figure 2 have a jump of 1–5% at $k_p a = 0.45 - 0.8$, depending on the material. This is due to a change of mesh in the FE calculations for low frequencies [33], so the inaccuracies in the FEM results are expected to be at least of this order.

It is seen that for aluminium, with a low anisotropy index, the calculated phase velocity and attenuation by all methods are in agreement with FEM. However, as expected, the explicit expressions of the Rayleigh asymptote (both the present (R–P) and SOA (R–SOA) [32] methods) are valid only for low frequencies (roughly $ka < 0.4$) while the numerical calculations with the present method (N–P) are valid for higher frequencies (to about $ka = 1$). Figure 2*c* for aluminium shows that the attenuation errors for the present and stochastic methods are below 10% in their expected frequency range of validity. Going to the graphs in figure 2 for inconel and copper with higher anisotropy factors, the SOA and Born models lose their accuracy in the low and intermediate frequencies (around 30% error for the attenuation), while both the explicit expression and the numerical calculation of the present approach have a good agreement with FEM in the expected frequency ranges (roughly less than 10% error for the attenuation). This indicates the advantage of the present method for high anisotropic polycrystals in comparison with the other analytical methods, which seem to be limited to more or less low anisotropy. For lithium, which is extremely anisotropic, figure 2 shows that the present method gives a better agreement with the FE calculation in comparison with the SOA and Born models, but there is still not a good agreement between the results.

For the transverse phase velocity and attenuation, since the numerical calculations of the SOA and FEMs are carried out only for longitudinal waves in the literature, only the R–SOA and Born methods are compared with the present method (both the R–P and N–P methods). Figure 3 shows (*a*) normalized transverse phase velocity C_s/c_s and (*b*) normalized transverse attenuation $\alpha_s a$ versus normalized frequency $k_s a$ for aluminium, inconel, copper and lithium, evaluated using the R–P method (dashed black lines), the N–P method (solid blue lines), the R–SOA method (dash-dotted black lines) and the Born method (dashed green lines). Similarly as in figure 2, for aluminium with a low anisotropy factor, the present and stochastic methods are in agreement with each other, while by increasing the degree of anisotropy the difference becomes substantial.

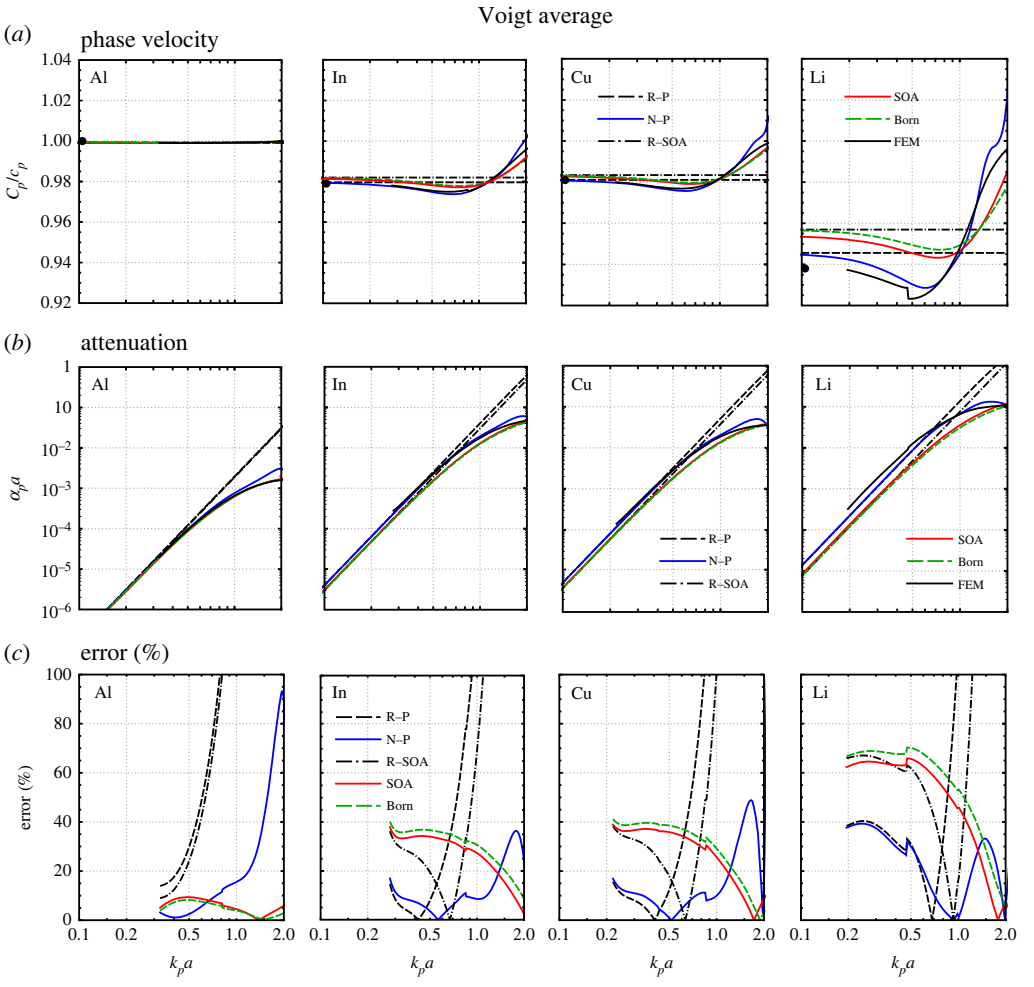

Figure 2. (*a*) Normalized phase velocity C_p/c_p, (*b*) normalized attenuation $\alpha_p a$ versus normalized frequency $k_p a$ for longitudinal waves evaluated by the Rayleigh asymptote of the present method, R–P (dashed black lines), numerical evaluation of the present method, N–P (solid blue lines), the Rayleigh asymptote of the SOA method, R–SOA (dash-dotted black lines) and the Born approximation of the FFA method, Born (dashed green lines), compared with numerical FEM results (solid black lines) in four cubic polycrystals with $A > 1$ in the order of anisotropy degree (Al, In, Cu and Li) and with the present average for the matrix properties. The correspondence with FEM for all methods are shown in (*c*) as attenuation error (%) with respect to FEM results ($|\alpha - \alpha_{\mathrm{FEM}}|/\alpha_{\mathrm{FEM}}$) as a function of normalized frequency. Also, the leftmost solid black points in (*a*) are quasi-static FEM results.

Looking at figures 2 and 3*a*, it can be observed that for aluminium polycrystal the normalized phase velocities at low frequencies (normalized quasi-static phase velocity) are equal to unity with an accuracy better than 0.1%, and this indicates that the matrix phase velocity calculated by the Voigt average (Voigt phase velocity) is a good estimation of the quasi-static effective phase velocity for aluminium polycrystals. In inconel and copper with a higher degree of anisotropy, the difference between the quasi-static effective phase velocity and the Voigt phase velocity increases to nearly 2% and 5% for the longitudinal and transverse phase velocities, respectively. This difference increases to nearly 5% and 12% for the longitudinal and transverse phase velocities of lithium, respectively. This is an indication that the Voigt average is not a proper estimation of the matrix properties of strongly anisotropic polycrystals, specifically for lithium with such a

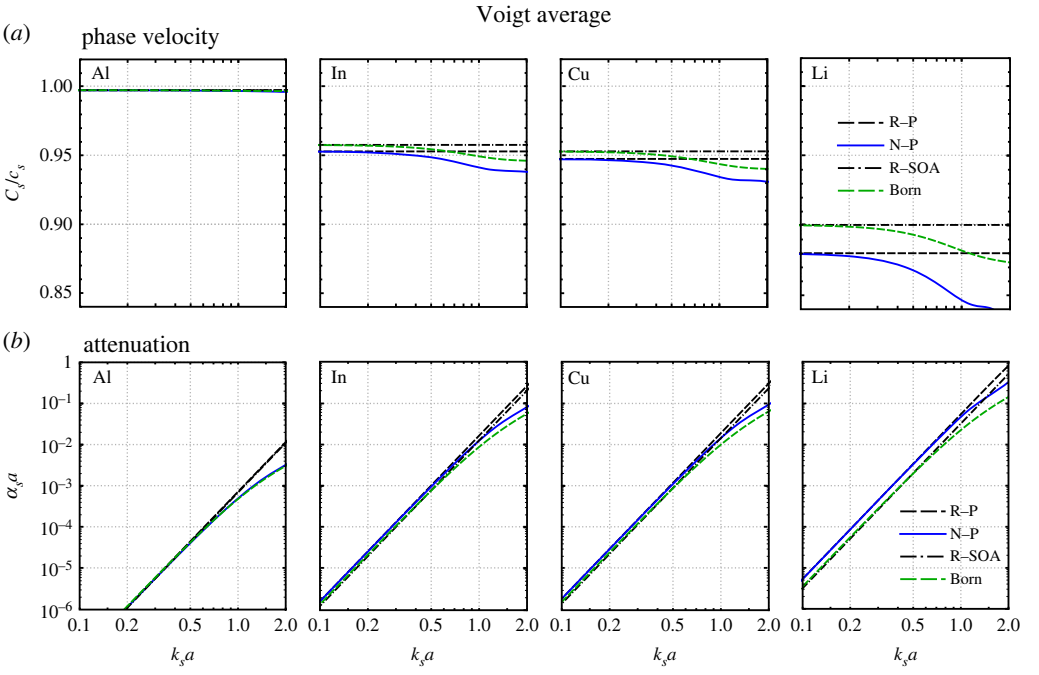

Figure 3. (*a*) Normalized phase velocity C_s/c_s and (*b*) normalized attenuation $\alpha_s a$ versus normalized frequency $k_s a$ for transverse waves evaluated by the Rayleigh asymptote of the present method, R–P (dashed black lines), numerical evaluation of the present method, N–P (solid blue lines), the Rayleigh asymptote of the SOA method, R–SOA (dash-dotted black lines) and the Born approximation of the FFA method, Born (dashed green lines), for four cubic polycrystals with $A > 1$ in the order of anisotropy degree (Al, In, Cu and Li) and with the Voigt average for the matrix properties.

high degree of anisotropy. Therefore, the effective phase velocity and attenuation are studied by considering the present average for the matrix properties.

As in figure 2, figure 4 shows (*a*) normalized longitudinal phase velocity C_p/c_p, (*b*) normalized longitudinal attenuation $\alpha_p a$ and (*c*) error of the attenuation with respect to FE results versus normalized frequency $k_p a$ for the four cubic polycrystals, this time with the present average for the matrix properties as stated in table 2. For each material, the phase velocity and attenuation are calculated with the R–P method (dashed black lines), the N–P method (solid blue lines), the R–SOA method (dash-dotted black lines), and the Born method (dashed green lines) and compared with FEM results (solid black lines and the leftmost solid black points in (*a*)). In figure 4*a*, it can be observed that the normalized quasi-static phase velocity for the present method is equal to unity as this was the criterion for defining the present average for the matrix properties.

A comparison of figures 2 and 4 shows the effect of the matrix properties on the attenuation and phase velocity of the polycrystalline materials. For the presents N–P and R–P methods there is a strong increase in the accuracy of both the phase velocity and attenuation as compared to FEM, except that the Rayleigh method (R–P) is only valid for low enough frequencies. Thus the errors in attenuation are reduced at the lowest frequencies from about 40% to less than 10%. However, for the R–SOA and Born methods the accuracy of the attenuation is strongly increased, whereas the phase velocity loses accuracy. These results are somewhat contradictory in that it is expected that the errors in phase velocity and attenuation should follow a similar trend. It thus seems that it is not a good idea to use the present average with the R–SOA and Born methods.

For the transverse waves, figure 5*a* shows normalized transverse phase velocity C_s/c_s and normalized transverse attenuation (figure 5*b*) $\alpha_s a$ versus normalized frequency $k_s a$ for aluminium,

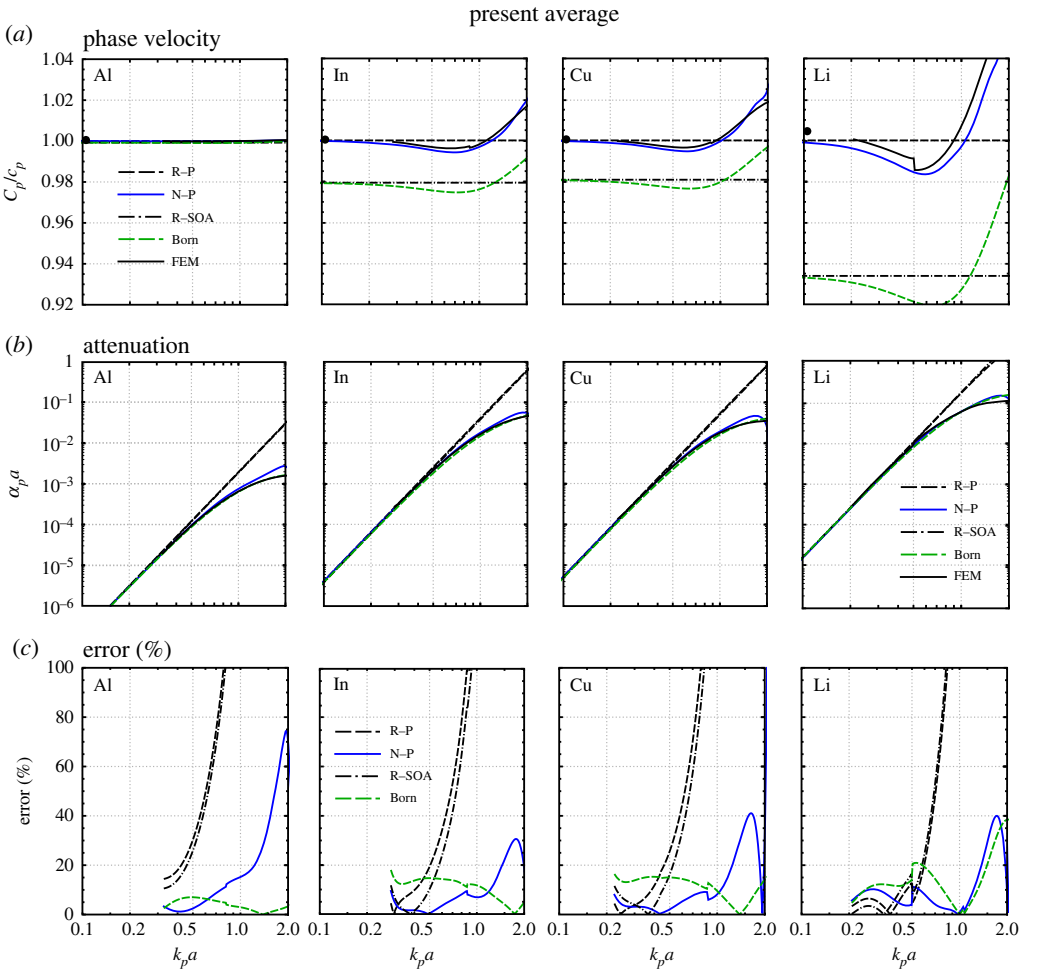

Figure 4. (*a*) Normalized phase velocity C_p/c_p, (*b*) normalized attenuation $\alpha_p a$ versus normalized frequency $k_p a$ for longitudinal waves evaluated by the Rayleigh asymptote of the present method, R–P (dashed black lines), numerical evaluation of the present method, N–P (solid blue lines), the Rayleigh asymptote of the SOA method, R–SOA (dash-dotted black lines), and the Born approximation of the FFA method, Born (dashed green lines), compared with numerical FEM results (solid black lines) in four cubic polycrystals with $A > 1$ in the order of anisotropy degree (Al, In, Cu and Li) and with the present average for the matrix properties. The correspondence with FEM for all methods are shown in (*c*) as attenuation error (%) with respect to FEM results ($|\alpha - \alpha_{\mathrm{FEM}}|/\alpha_{\mathrm{FEM}}$) as a function of normalized frequency. Also, the leftmost solid black points in (*a*) are quasi-static FEM results.

inconel, copper and lithium, evaluated using the present average for the matrix, by the R–P method (dashed black lines), the N–P method (solid blue lines), the R–SOA method (dash-dotted black lines) and the Born method (dashed green lines). As discussed for the longitudinal waves, the R–SOA and Born calculations of the phase velocity are unreliable using the present average (see figure 5*a*). But, with the present average, the attenuation calculated by the present, R–SOA and Born methods are in agreement with each other for all materials (see figure 5*b*).

9. Concluding remarks

In the present paper, the elastic wave scattering by an anisotropic sphere with cubic symmetry in an isotropic surrounding is investigated. Using spherical coordinates, expansions in vector spherical harmonics in the angular coordinates and powers in the radial coordinate lead to

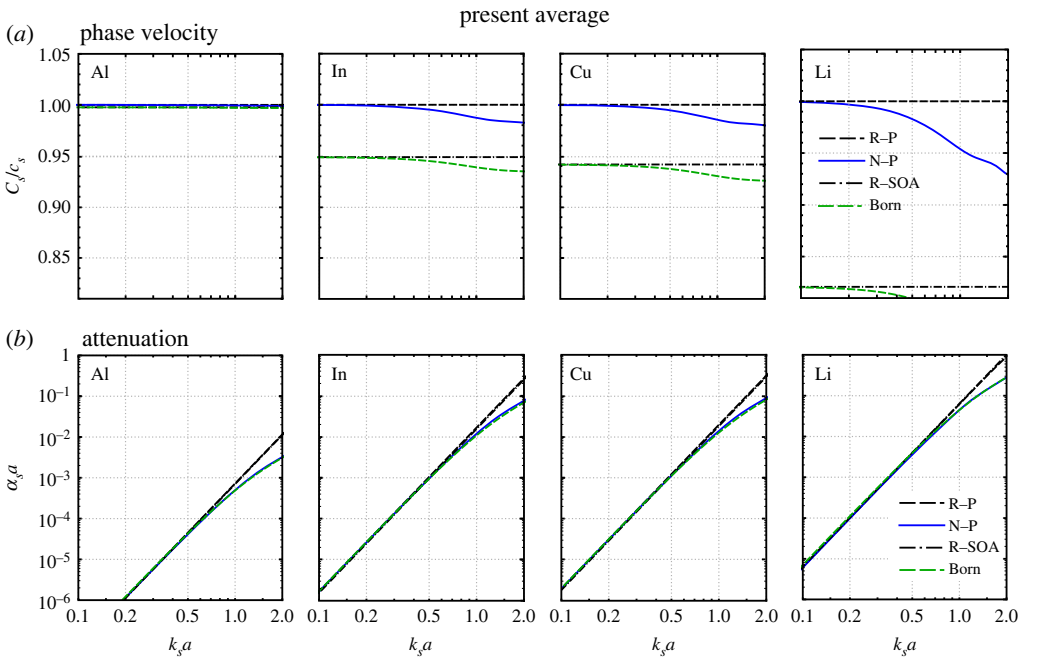

Figure 5. (*a*) Normalized phase velocity C_s/c_s, (*b*) normalized attenuation $\alpha_s a$ versus normalized frequency $k_s a$ for transverse waves evaluated by the Rayleigh asymptote of the present method, R–P (dashed black lines), numerical evaluation of the present method, N–P (solid blue lines), the Rayleigh asymptote of the SOA method, R–SOA (dashdotted black lines), and the Born approximation of the FFA method, Born (dashed green lines), for four cubic polycrystals with $A > 1$ in the order of anisotropy degree (Al, In, Cu and Li), and with the present average for the matrix properties.

recursion relations among the expansion coefficients. The boundary conditions on the sphere then lead to the determination of the elements of the transition (**T**) matrix. In the low frequency limit the leading order elements are given explicitly in simple form. Monopole, dipole and quadrupole elements all contribute and the dipole elements only depend on the density of the sphere and are, in fact, the same as for an isotropic sphere. The monopole and quadrupole elements, on the other hand, only depend on the elasticity of the sphere.

As an application the attenuation and phase velocity of single phase polycrystalline materials with grains with cubic anisotropy are calculated using the simple Foldy theory and explicit expressions are given for low frequencies. In the literature, the Voight average has mostly been employed to determine the unperturbed elasticity constants of the material, but it is shown that for highly anisotropic materials, e.g. lithium, this does not work very well. Instead a new approach is introduced which is shown to work much better. Comparisons are performed with other theories and with numerical FEM computations from the literature and for low frequencies and high anisotropy it is seen that the present method gives a much better agreement with FEM than the other methods. Some of the other methods, on the other hand, are not limited to low frequencies.

The present method is limited to low frequencies due to several factors. The explicit form of the **T** matrix elements used are only accurate for low frequencies, although it is shown that a numerical computation of more **T** matrix elements extends the frequency range somewhat, but at the cost of a much more complicated approach. Use of the Foldy theory is a limitation, but this might possibly be improved if more refined multiple scattering theories are used. The present approach is limited to spherical grains and this is adequate for low frequencies where the scattering is predominantly a volume effect, but is otherwise questionable.

The present methods can be extended in several ways. Other classes of anisotropy can be investigated, orthotropic materials are of particular interest. Only spheres of the same size are used in the present approach but within the Foldy approach it should be straightforward to consider a distribution in size of the spheres. It should also be possible to consider spheres of two or more different materials, e.g. a duplex material.

Data accessibility. The data are provided in electronic supplementary material [37].

Authors' contributions. A.J.: formal analysis, methodology, software, writing—original draft; P.D.F.: funding acquisition, methodology, supervision, writing—review and editing; A.B.: conceptualization, funding acquisition, methodology, supervision, writing—review and editing.

All authors gave final approval for publication and agreed to be held accountable for the work performed therein.

Conflict of interest declaration. The authors declare the following financial interests/personal relationships which may be considered as potential competing interests: Anders Bostrom reports financial support was provided by Swedish Research Council. Anders Bostrom reports a relationship with Swedish Research Council that includes: funding grants.

Funding. The present project is funded by the Swedish Research Council (grant no.2017-03958) and this is gratefully acknowledged.

Acknowledgements. The FE and SOA results that are used as a comparison have very kindly been provided by Prof. M. Lowe and Dr M. Huang, Imperial College, London.

References

1. Mow CC, Pao YH. 1973 *The diffraction of elastic waves and dynamic stress concentrations*. New York, NY: Crane-Russack.
2. de Hoop A. 1995 *Handbook of radiation and scattering of waves: acoustic waves I: fluids, elastic waves in solids, electromagnetic waves*. San Diego, CA: Academic Press.
3. Varadan VV, Lakhtakia A, Varadan VK. 1991 *Field representations and introduction to scattering*. Amsterdam, The Netherlands: North-Holland.
4. Martin PA, Berger JR. 2001 Waves in wood: free vibrations of a wooden pole. *J. Mech. Phys. Solids* **49**, 1155–1178. (doi:10.1016/S0022-5096(00)00068-5)
5. Hasheminejad SM, Maleki M. 2008 Acoustic resonance scattering from a submerged anisotropic sphere. *Acoust. Phys.* **54**, 168–179. (doi:10.1134/S1063771008020048)
6. Norris AN, Shuvalov AL. 2012 Elastodynamics of radially inhomogeneous spherically anisotropic elastic materials in the Stroh formalism. *Proc. R. Soc. A* **468**, 467–484. (doi:10.1098/rspa.2011.0463)
7. Guild MD, Alù A, Haberman MR. 2014 Cloaking of an acoustic sensor using scattering cancellation. *Appl. Phys. Lett.* **105**, 023510 (doi:10.1063/1.4890614)
8. Chung MY. 2019 Stress amplification/shielding phenomena of spherically anisotropic and radially inhomogeneous linear elastic hollow spheres. *Q. J. Mech. Appl. Math.* **72**, 535–544. (doi:10.1093/qjmam/hbz017)
9. Wan C, Li H. 2012 Analytical method and semianalytical method for analysis of scattering by anisotropic sphere: a review. *Int. J. Antennas Propag.* **2012**, 782320 (doi:10.1155/2012/782320)
10. Doicu A. 2003 Null-field method to electromagnetic scattering from uniaxial anisotropic particles. *Opt. Commun.* **218**, 11–17. (doi:10.1016/S0030-4018(03)01164-7)
11. Wang JJ, Han YP, Han L, Cui ZW. 2014 Electromagnetic scattering from gyroelectric anisotropic particle by the T-matrix method. *J. Quant. Spectrosc. Radiat. Transf.* **135**, 20–29. (doi:10.1016/j.jqsrt.2013.12.009)
12. Boström A. 2015 Scattering by an anisotropic circle. *Wave Motion* **57**, 239–244. (doi:10.1016/j.wavemoti.2015.04.007)
13. Boström A. 2018 Scattering of in-plane elastic waves by an anisotropic circle. *Q. J. Mech. Appl. Math.* **71**, 139–155. (doi:10.1093/qjmam/hbx029)
14. Jafarzadeh A, Folkow PD, Boström A. 2020 Scattering of elastic SH waves by transversely isotropic sphere. In *Proc. of the Int. Conf. on Structural Dynamic, EURODYN, Athens, Greece* (streamed), 23–26 November, vol. 2, pp. 2782–2797. Athens, Greece: NTUA.
15. Jafarzadeh A, Folkow PD, Boström A. 2022 Scattering of elastic waves by a transversely isotropic sphere and ultrasonic attenuation in hexagonal polycrystalline materials. *Wave Motion* **112**, 102963 (doi:10.1016/j.wavemoti.2022.102963)

16. Martin PA. 2006 *Multiple scattering: interaction of time-harmonic waves with N obstacles*, vol. 107. Cambridge, UK: Cambridge University Press.
17. Foldy LL. 1945 The multiple scattering of waves. I. General theory of isotropic scattering by randomly distributed scatterers. *Phys. Rev.* **67**, 107–119. (doi:10.1103/PhysRev.67.107)
18. Mal AK, Knopoff L. 1967 Elastic wave velocities in two-component systems. *IMA J. Appl. Math.* **3**, 376–387. (doi:10.1093/imamat/3.4.376)
19. Gubernatis JE, Domany E. 1984 Effects of microstructure on the speed and attenuation of elastic waves in porous materials. *Wave Motion* **6**, 579–589. (doi:10.1016/0165-2125(84)90048-9)
20. Datta SK, Ledbetter HM, Shindo Y, Shah AH. 1988 Phase velocity and attenuation of plane elastic waves in a particle-reinforced composite medium. *Wave Motion* **10**, 171–182. (doi:10.1016/0165-2125(88)90042-X)
21. Boström A, Olsson P, Datta SK. 1992 Effective plane wave propagation through a medium with spheroidal inclusions surrounded by thin interface layers. *Mech. Mater.* **14**, 59–66. (doi:10.1016/0167-6636(92)90018-9)
22. Stanke FE, Kino GS. 1984 A unified theory for elastic wave propagation in polycrystalline materials. *J. Acoust. Soc. Am.* **75**, 665–681. (doi:10.1121/1.390577)
23. Weaver RL. 1990 Diffusivity of ultrasound in polycrystals. *J. Mech. Phys. Solids* **38**, 55–86. (doi:10.1016/0022-5096(90)90021-U)
24. Rokhlin SI, Li J, Sha G. 2015 Far-field scattering model for wave propagation in random media. *J. Acoust. Soc. Am.* **137**, 2655–2669. (doi:10.1121/1.4919333)
25. Yang L, Li J, Rokhlin SI. 2013 Ultrasonic scattering in polycrystals with orientation clusters of orthorhombic crystallites. *Wave Motion* **50**, 1283–1302. (doi:10.1016/j.wavemoti.2013.06.003)
26. Yang L, Lobkis OI, Rokhlin SI. 2011 Explicit model for ultrasonic attenuation in equiaxial hexagonal polycrystalline materials. *Ultrasonics* **51**, 303–309. (doi:10.1016/j.ultras.2010.10.002)
27. Li J, Rokhlin SI. 2016 Elastic wave scattering in random anisotropic solids. *Int. J. Solids Struct.* **78**, 110–124. (doi:10.1016/j.ijsolstr.2015.09.011)
28. Boström A, Ruda A. 2019 Ultrasonic attenuation in polycrystalline materials in 2D. *J. Nondestruct. Eval.* **38**, 1–6. (doi:10.1007/s10921-019-0590-9)
29. Van Pamel A, Brett CR, Huthwaite P, Lowe MJS. 2015 Finite element modelling of elastic wave scattering within a polycrystalline material in two and three dimensions. *J. Acoust. Soc. Am.* **138**, 2326–2336. (doi:10.1121/1.4931445)
30. Van Pamel A, Sha G, Rokhlin SI, Lowe MJS. 2017 Finite-element modelling of elastic wave propagation and scattering within heterogeneous media. *Proc. R. Soc. A* **473**, 20160738 (doi:10.1098/rspa.2016.0738)
31. Van Pamel A, Sha G, Lowe MJS, Rokhlin SI. 2018 Numerical and analytic modelling of elastodynamic scattering within polycrystalline materials. *J. Acoust. Soc. Am.* **143**, 2394–2408. (doi:10.1121/1.5031008)
32. Sha G, Huang M, Lowe MJS, Rokhlin SI. 2020 Attenuation and velocity of elastic waves in polycrystals with generally anisotropic grains: analytic and numerical modeling. *J. Acoust. Soc. Am.* **147**, 2442–2465. (doi:10.1121/10.0001087)
33. Huang M, Sha G, Huthwaite P, Rokhlin SI, Lowe MJS. 2020 Maximizing the accuracy of finite element simulation of elastic wave propagation in polycrystals. *J. Acoust. Soc. Am.* **148**, 1890–1910. (doi:10.1121/10.0002102)
34. Huang M, Huthwaite P, Rokhlin SI, Lowe MJS. 2022 Finite-element and semi-analytical study of elastic wave propagation in strongly scattering polycrystals. *Proc. R. Soc. A* **478**, 20210850 (doi:10.1098/rspa.2021.0850)
35. Boström A. 1980 Scattering by a smooth elastic obstacle. *J. Acoust. Soc. Am.* **67**, 1904–1913. (doi:10.1121/1.384455)
36. Waterman PC. 1976 Matrix theory of elastic wave scattering. *J. Acoust. Soc. Am.* **60**, 567–580. (doi:10.1121/1.381130)
37. Jafarzadeh A, Folkow PD, Boström A.2023 Scattering of elastic waves by a sphere with cubic anisotropy with application to attenuation in polycrystalline materials. Figshare. (doi:10.6084/m9.figshare.c.6589814)